ARTICLE

doi:10.1038/nature24628

Salt–responsive gut commensal modulates T_H17 axis and disease

Nicola Wilck[1,2,3,4,5], Mariana G. Matus[6,7], Sean M. Kearney[6], Scott W. Olesen[6], Kristoffer Forslund[8], Hendrik Bartolomaeus[1,2,3,4], Stefanie Haase[9], Anja Mähler[1,5], András Balogh[1,2,3,4,5], Lajos Markó[1,2,3,4,5], Olga Vvedenskaya[3,10,11], Friedrich H. Kleiner[1], Dmitry Tsvetkov[1,2], Lars Klug[1,5], Paul I. Costea[8], Shinichi Sunagawa[8,12], Lisa Maier[13], Natalia Rakova[1,9], Valentin Schatz[14], Patrick Neubert[14], Christian Frätzer[15], Alexander Krannich[5], Maik Gollasch[1,2,3], Diana A. Grohme[16], Beatriz F. Côrte-Real[17], Roman G. Gerlach[18], Marijana Basic[19], Athanasios Typas[13], Chuan Wu[20], Jens M. Titze[21], Jonathan Jantsch[14], Michael Boschmann[1,5], Ralf Dechend[1,2,5], Markus Kleinewietfeld[16,17,22], Stefan Kempa[3,5,10], Peer Bork[3,8,23,24], Ralf A. Linker[9]§, Eric J. Alm[6]§ & Dominik N. Müller[1,2,3,4,5]§

A Western lifestyle with high salt consumption can lead to hypertension and cardiovascular disease. High salt may additionally drive autoimmunity by inducing T helper 17 (T_H17) cells, which can also contribute to hypertension. Induction of T_H17 cells depends on gut microbiota; however, the effect of salt on the gut microbiome is unknown. Here we show that high salt intake affects the gut microbiome in mice, particularly by depleting *Lactobacillus murinus*. Consequently, treatment of mice with *L. murinus* prevented salt–induced aggravation of actively induced experimental autoimmune encephalomyelitis and salt–sensitive hypertension by modulating T_H17 cells. In line with these findings, a moderate high–salt challenge in a pilot study in humans reduced intestinal survival of *Lactobacillus* spp., increased T_H17 cells and increased blood pressure. Our results connect high salt intake to the gut–immune axis and highlight the gut microbiome as a potential therapeutic target to counteract salt–sensitive conditions.

High salt content in the Western diet has been implicated in numerous disorders[1], particularly in cardiovascular disease[2]. Guidelines[3,4] and public initiatives recommend reducing salt intake, but an improved mechanistic understanding is needed. The deleterious effect of a high salt diet (HSD) on cardiovascular health is driven by arterial hypertension and associated with increased morbidity and mortality[2,5]. Thus far, most studies have focused on the role of the kidneys, the sympathetic nervous system and direct effects on the vasculature[6]. However, some studies implicate the immune system in these processes[7], linking pro-inflammatory T cells to the development of hypertension[8]. In particular, interleukin-17A (IL-17A)-producing $CD4^+$ T_H17 cells may promote hypertension[9,10]. T_H17 cells play a deleterious role in autoimmune diseases. Studies have recently demonstrated that the generation of pathogenic T_H17 cells could be promoted by a high salt environment. Consequently, a HSD boosts T_H17 generation and exacerbates actively induced experimental autoimmune encephalomyelitis (EAE)[11,12], as a prototypic autoimmune disease driven by T_H17 cells[13]. Active myelin oligodendrocyte glycoprotein $(MOG)_{35–55}$-induced EAE is a disease model that recapitulates many aspects of multiple sclerosis, although differing from transgenic EAE models in several aspects of T-cell function[14]. The intestine is exposed to varying salt loads of ingested foods, yet the interaction between HSD and the gut microbiome has not been thoroughly investigated. Gut microbes are known to respond to fluctuations in dietary composition[15], leading to transient or persistent alterations in the gut microbiome[16]. Diet-induced shifts in microbiome composition may have profound effects on the host, especially on T cells[17]. T_H17 cells are particularly affected by the abundance of specific commensal bacteria[18]. We investigated the influence of high-salt challenges on the gut microbiome and the immune system, and determined the implications of HSD for hypertension and autoimmunity.

High salt decreases *Lactobacillus* in mice

To determine the effect of a HSD on the composition of the gut microbiome, we analysed faecal pellets from FVB/N mice that were fed a normal salt diet (NSD) or HSD by 16S ribosomal DNA (rDNA) gene sequencing. Both diets were equally well-tolerated, indicated by similar body weight and food intake (Extended Data Fig. 1a, b). HSD-fed mice had a significantly higher fluid and salt intake than NSD-fed mice (Extended Data Fig. 1c–f), but similar intestinal transit (Extended Data Fig. 1g). The overall microbial composition (based on operational taxonomic units, OTUs, assigned using the Ribosomal Database Project[19]) showed no obvious pattern shifts between

[1]Experimental and Clinical Research Center, a joint cooperation of Max-Delbrück Center for Molecular Medicine and Charité-Universitätsmedizin Berlin, 13125 Berlin, Germany. [2]Charité-Universitätsmedizin Berlin, 10117 Berlin, Germany. [3]Max-Delbrück Center for Molecular Medicine in the Helmholtz Association, 13125 Berlin, Germany. [4]DZHK (German Centre for Cardiovascular Research), partner site Berlin, Germany. [5]Berlin Institute of Health (BIH), Berlin, Germany. [6]Center for Microbiome Informatics and Therapeutics, and Department of Biological Engineering, Massachusetts Institute of Technology, Cambridge, Massachusetts 02139, USA. [7]Computational and Systems Biology Program, Massachusetts Institute of Technology, Cambridge, Massachusetts 02139, USA. [8]European Molecular Biology Laboratory, Structural and Computational Biology Unit, 69117 Heidelberg, Germany. [9]Department of Neurology, Friedrich-Alexander-University Erlangen-Nuremberg, 91054 Erlangen, Germany. [10]Integrative Proteomics and Metabolomics Platform, Berlin Institute for Medical Systems Biology BIMSB, 13125 Berlin, Germany. [11]Berlin School of Integrative Oncology, Charité University Medicine Berlin, Berlin, Germany. [12]Institute of Microbiology, ETH Zurich, 8092 Zurich, Switzerland. [13]European Molecular Biology Laboratory, Genome Biology Unit, 69117 Heidelberg, Germany. [14]Institute of Clinical Microbiology and Hygiene, University Hospital of Regensburg, University of Regensburg, 93053 Regensburg, Germany. [15]Lipidomix GmbH, 13125 Berlin, Germany. [16]Translational Immunology, Department of Clinical Pathobiochemistry, Medical Faculty Carl Gustav Carus, Technical University of Dresden, 01307 Dresden, Germany. [17]VIB Laboratory of Translational Immunomodulation, VIB Center for Inflammation Research (IRC), Hasselt University, Campus Diepenbeek, 3590 Diepenbeek, Belgium. [18]Project Group 5, Robert Koch Institute, 38855 Wernigerode, Germany. [19]Hannover Medical School, Institute for Laboratory Animal Science and Central Animal Facility, 30625 Hannover, Germany. [20]Experimental Immunology Branch, National Cancer Institute, US National Institutes of Health, Bethesda, Maryland, USA. [21]Division of Clinical Pharmacology, Vanderbilt University School of Medicine, Nashville, Tennessee, USA. [22]Center for Regenerative Therapies Dresden (CRTD), 01307 Dresden, Germany. [23]Molecular Medicine Partnership Unit, University of Heidelberg and European Molecular Biology Laboratory, 69120 Heidelberg, Germany. [24]Department of Bioinformatics, Biocenter, University of Würzburg, 97074 Würzburg, Germany.
§These authors jointly supervised this work.

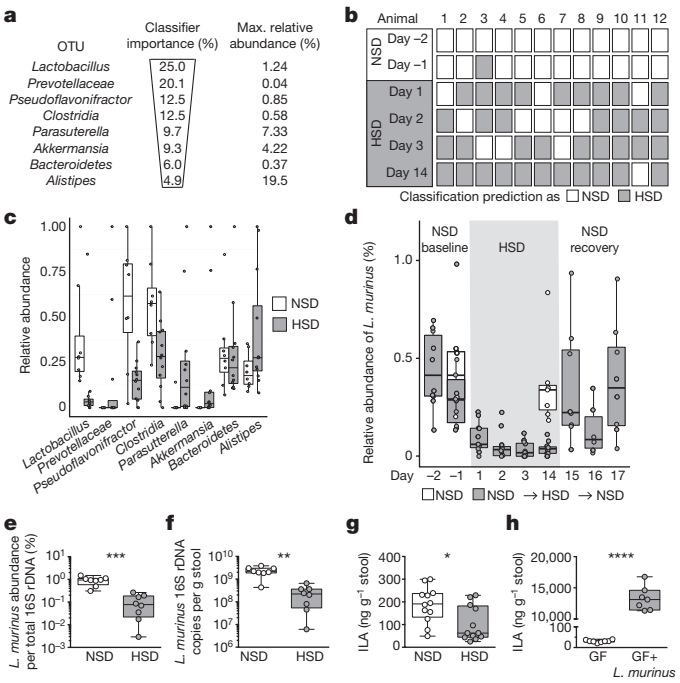

Figure 1 | HSD alters the faecal microbiome and depletes *Lactobacillus* in mice. a, AdaBoost identified eight 16S rDNA OTUs distinguishing samples of NSD-fed mice from HSD-fed mice. **b**, Classifier accuracy per mouse and diet. **c**, Relative OTU abundances on HSD day 14 ($n = 12$ mice; $n = 8$ NSD control mice). **d**, *Lactobacillus* abundance over time. Samples with >1% are not shown. **e**, **f**, *L. murinus* qPCR ($n = 8$ mice). **g**, Faecal ILA, $n = 12$ mice per group. **h**, Faecal ILA in gnotobiotic mice ($n = 8$ germ-free; $n = 7$ *L. murinus*-monocolonized mice). Box plots show median and interquartile range (IQR), whiskers are 1.5× IQR (**c**, **d**) or minimum and maximum values (**e**–**h**). $^*P < 0.05$; $^{**}P < 0.01$; $^{***}P < 0.001$; $^{****}P < 0.0001$; paired two-tailed *t*-test (**f**), Wilcoxon signed-rank test (**g**), unpaired two-tailed *t*-test (**h**).

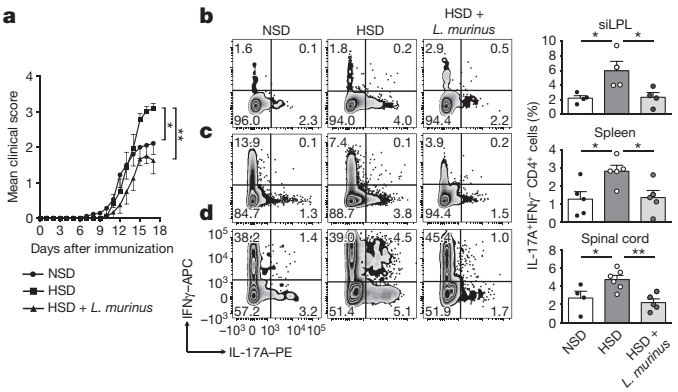

Figure 2 | *L. murinus* prevents HSD-induced exacerbation of EAE and reduces the number of T_H17 cells. a, Mean disease scores of $MOG_{35–55}$ EAE mice fed with a NSD ($n = 9$), HSD ($n = 11$) or HSD with *L. murinus* ($n = 6$). **b**, siLPL (day 3 after immunization) analysed by flow cytometry for $CD4^+IL\text{-}17A^+IFN\gamma^-$ cells ($n = 4$). **c**, **d**, Spleens (**c**; $n = 5$) and spinal cords (**d**; NSD, $n = 4$; HSD, $n = 6$; HSD with *L. murinus*, $n = 5$; day 17 after immunization) were analysed as in **b**. Representative plots are shown on the left, quantification on the right. Data are mean ± s.e.m.; circles represent individual mice. $^*P < 0.05$; $^{**}P < 0.01$; one-way ANOVA and post hoc Tukey's test (**c**), Kruskal–Wallis and Dunn's post hoc test for (**a**, **b**, **d**). *n* indicates the number of mice per group.

HSD- and NSD-fed mice (Extended Data Figs 2a, b, 3a). Although analyses using Jensen–Shannon divergence indicated differences between bacterial communities of HSD and NSD-fed mice, these differences were not confirmed by Bray–Curtis or UniFrac[20] metrics (data not shown). Bacterial load was not significantly different between NSD- and HSD-fed mice (Extended Data Fig. 3b), but several OTUs were significantly decreased after a HSD on day 14, including species of the genera *Lactobacillus*, *Oscillibacter*, *Pseudoflavonifractor*, *Clostridium* XIVa, *Johnsonella* and *Rothia*, whereas others increased after a HSD, for example, *Parasutterella* spp. (Extended Data Fig. 3c). Notably, analysis of faecal metabolites from central carbon and nitrogen metabolic pathways by gas-chromatography–mass spectrometry (GC–MS) showed clear differences between the two groups (Extended Data Fig. 3d–g). The absence of large-scale taxonomic differences was unexpected, given the differences in metabolites, but is consistent with the fact that the two diets are identical in energy content and only differ in salt content. To identify the specific bacterial OTUs that did change across diet, we used a sensitive machine learning approach. An AdaBoost classifier trained to distinguish NSD from HSD samples on day 14 of the treatment identified 8 OTUs with nontrivial feature importance (Fig. 1a, c) with 92% accuracy (Fig. 1b). These OTUs varied in maximum relative abundance (from 0.04% to 19.5%) and responded differently to the HSD (Fig. 1a, c). OTUs identified as most important were consistent across different cross-validation runs and across different algorithms (Extended Data Fig. 4a). The most important OTU (25% feature importance) was a member of the genus *Lactobacillus* and was depleted after HSD (Fig. 1d). Other features included OTUs from *Prevotellaceae*, *Pseudoflavonifractor*, *Clostridia*, *Parasutterella*, *Akkermansia*, *Bacteroidetes* and *Alistipes* (Fig. 1a, c and Extended Data Fig. 4b). *Lactobacillus* depletion showed a quick onset that was detectable one day after the initiation of the HSD, remaining at low levels during the HSD with the lowest abundance on day 14. When the mice were returned to a NSD, the *Lactobacillus* OTU abundance returned to baseline levels (Fig. 1d).

Because the *Lactobacillus* OTU was the bacterial group most strongly associated with high salt, we isolated a *Lactobacillus* strain from mouse faeces. The 16S rDNA sequence of the isolate shared 100% identity with the V4–V5 16S region of the OTU described above, and was identified as *L. murinus*. We confirmed the decrease in abundance of this strain after a HSD using qPCR (Fig. 1e, f). Genome sequencing of the isolate showed 93% similarity to two published *L. murinus* genomes[21,22] (Extended Data Fig. 5a). Notably, there are no strains of *L. murinus* known to be native to the human microbiota; the closest 16S sequence in the human gut microbiota matches with less than 90% nucleotide identity (Extended Data Fig. 5b). The prevalence of different *Lactobacillus* species varies in humans; each species is present in 0.5–22% of subjects in the MetaHIT[23] subcohort of Danish subjects (Extended Data Fig. 5b).

Next, we cultured *L. murinus*, human-associated *Lactobacillus* species and non-related control strains *in vitro* and tested their growth under increasing NaCl concentrations. Half maximal growth inhibition (IC_{50}) of *L. murinus* occurred at comparable NaCl concentrations under aerobic and anaerobic culture conditions (Extended Data Fig. 5c, d). NaCl inhibited the growth of several human isolates at slightly lower concentrations, with the exception of *Lactobacillus salivarius* (Extended Data Fig. 5e, f). However, not all strains tested were similarly salt-sensitive. For instance, *Akkermansia muciniphila*, identified by the classifier and increasing in faecal abundance upon HSD, and *Escherichia coli* had higher salt tolerances (Extended Data Fig. 5d, g). Notably, *in vivo* colonic faecal sodium concentrations in HSD-fed mice are comparable to growth-inhibitory NaCl concentrations *in vitro* (0.252 M for HSD versus 0.133 M for NSD).

Because *Lactobacillus* species are known to metabolize tryptophan to indole metabolites[24], we speculated that a HSD would also reduce faecal indoles. Indeed, HSD significantly reduced faecal levels of indole-3-lactic acid (ILA, Fig. 1g) and indole-3-acetic acid (IAA, Extended Data Fig. 6a), whereas indole-3-carboxaldehyde was unchanged (IAld, Extended Data Fig. 6b). In contrast to germ-free controls, mice monocolonized with the *L. murinus* isolate exhibited significantly higher fecal ILA, IAA and IAld, which indicates that *L. murinus* is capable of producing these indoles (Fig. 1h and Extended Data Fig. 6c, d).

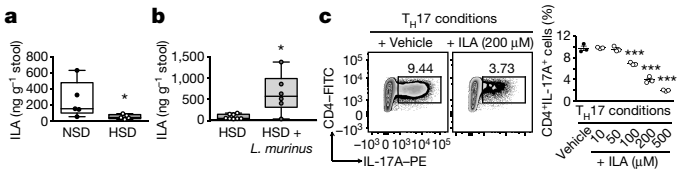

Figure 3 | Putative role for ILA. a, HSD reduces faecal ILA in MOG_{35-55} EAE mice ($n = 5$, day 10 after immunization). **b**, Faecal ILA in HSD-fed and *L. murinus*-treated mice ($n = 6$) compared to HSD-fed MOG_{35-55} EAE mice ($n = 8$), day 10 after immunization. Circles represent samples from individual mice. Box plots show median and IQR, whiskers are minimum and maximum values. $^*P < 0.05$; unpaired one-tailed *t*-test (**a**), Mann–Whitney *U*-test for (**b**). **c**, Naive mouse $CD4^+$ T cells cultured under T_H17-polarizing conditions in the presence (+ILA) or absence (+vehicle) of ILA, analysed for IL-17A ($n = 3$ biological replicates per group). Data are mean ± s.e.m., one representative out of two independent experiments is shown. $^{***}P < 0.001$ versus vehicle; one-way ANOVA and Tukey's post hoc test.

L. murinus ameliorates active EAE

The importance of the gut microbiome has recently been recognized for multiple sclerosis[25] and EAE[26]. The suppression of *L. murinus* by HSD prompted us to investigate whether oral administration of *L. murinus* ameliorates HSD-induced exacerbation of actively induced MOG_{35-55} EAE.

We relied on a daily gavage protocol to maintain *L. murinus* abundance and faecal indole metabolites during HSD. Body weight and disease incidence were similar in all groups. Mice on a HSD displayed an exacerbated disease course (Fig. 2a and Extended Data Fig. 7a). *L. murinus* supplementation during HSD and NSD feeding ameliorated the disease (Fig. 2a and Extended Data Fig. 7a, b). Similar results were observed when HSD-fed mice were treated with *Lactobacillus reuteri* (Extended Data Fig. 7c). We analysed $CD4^+$ small intestinal lamina propria lymphocytes (siLPL) producing IL-17A by flow cytometry on day 3 after MOG immunization when intestinal T_H17 cell expansion was at its maximum[27]. HSD-fed mice had a significantly higher frequency of T_H17 cells compared to NSD-fed mice, and this frequency was reduced in HSD-fed mice that concomitantly received *Lactobacillus murinus* (Fig. 2b). Flow cytometry analysis of splenocytes and spinal cord-infiltrating lymphocytes on day 17 after immunization revealed a significant reduction in T_H17 cells after treatment with *L. murinus* (Fig. 2c, d) and *L. reuteri* (Extended Data Fig. 7d, e) compared to HSD feeding alone. mRNA expression of *Il17a* and *Rorc* in spinal cord tissue was decreased after *L. murinus* treatment with a tendency towards lower *Csf2* levels (Extended Data Fig. 7f–h). The effect of HSD and *L. murinus* was mostly T_H17-specific, because interferon-γ (IFNγ)-producing $CD4^+$ lymphocytes were not affected in the siLPL, spleen or spinal cord (Extended Data Fig. 7i). Because we focused on actively induced MOG_{35-55} EAE, further studies are needed to extend the concept of HSD and *Lactobacillus* treatment in spontaneous EAE.

To elaborate on putative mechanisms for the modulation of T_H17 cells, we focused on faecal indole metabolites, which are known to improve actively induced EAE[28]. HSD significantly reduced faecal ILA, whereas concomitant *L. murinus* supplementation prevented this effect (Fig. 3a, b). A similar pattern was observed for faecal IAA and IAld (Extended Data Fig. 7j–m). Next, we investigated the effect of ILA on the differentiation of mouse T_H17 cells *in vitro*. ILA significantly reduced T_H17 polarization in a dose-dependent manner (Fig. 3c).

However, in MOG_{35-55}-immunized germ-free mice, HSD did not change T_H17 cell frequencies compared to NSD (Extended Data Fig. 8a, b), indicating a crucial role for intestinal bacteria in mediating the effect of a HSD on T_H17 cells. To corroborate the modulatory effects of *L. murinus*, we used segmented filamentous bacteria (SFB) as known inducers of intestinal T_H17 cells[18] and compared MOG_{35-55} immunization in gnotobiotic mice that had either only SFB (germ-free with SFB) or SFB and *L. murinus* (germ-free with SFB and *L. murinus*). As predicted, the presence or absence of *L. murinus* determined T_H17 cell frequencies in siLPL and colonic LPL (cLPL) (Extended Data Fig. 8c, d).

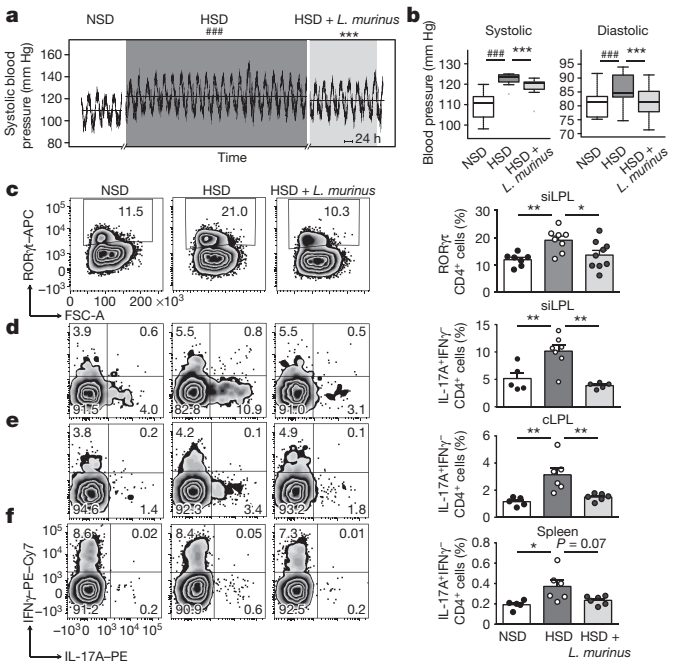

Figure 4 | *L. murinus* ameliorates salt-sensitive hypertension and reduces the number of T_H17 cells. Continuous blood pressure recordings in $n = 7$ FVB/N mice. **a**, **b**, Mean systolic pressures over time (**a**) and box plots of systolic and diastolic blood pressures (**b**). Box plots show median and IQR, whiskers are 1.5× IQR. $^{###}P < 0.001$ HSD versus NSD, $^{***}P < 0.001$ HSD with *L. murinus* versus HSD; linear mixed model. **c**, $CD4^+RORγt^+$ siLPL in mice fed a NSD ($n = 7$), HSD ($n = 8$) or HSD with *L. murinus* ($n = 9$). **d**–**f**, $CD4^+IL\text{-}17A^+IFNγ^-$ siLPL (**d**), cLPL (**e**) or splenocytes (**f**) out of the total number of $CD4^+$ cells in mice fed a NSD ($n = 5$), HSD ($n = 6$; siLPL, $n = 7$) and HSD with *L. murinus* ($n = 6$; siLPL, $n = 5$). Representative plots per group are shown, the quantification shows the mean ± s.e.m., circles represent individual mice. $^*P < 0.05$; $^{**}P < 0.01$; one-way ANOVA and post hoc Tukey's test (**c**, **e**, **f**), Kruskal–Wallis and post hoc Dunn's test (**d**).

L. murinus reduces salt-sensitive hypertension

Accumulating evidence suggests that T_H17 cells have a role in the genesis of hypertension[7]. Moreover, a recent meta-analysis provided preliminary support that *Lactobacillus*-rich probiotics might affect blood pressure in hypertensive subjects[29]. Therefore, we tested whether *L. murinus* treatment decreased experimental salt-sensitive hypertension.

Blood pressure increased over three weeks of HSD (Fig. 4a, b and Extended Data Fig. 9a). Concomitant daily treatment with *L. murinus* led to a significant reduction in systolic blood pressure and normalization of diastolic blood pressure (Fig. 4a, b and Extended Data Fig. 9b, c). *L. reuteri* was similarly effective, whereas the non-*Lactobacillus* strain *E. coli* Nissle 1917 was ineffective (Extended Data Fig. 9d–g).

We next asked whether *L. murinus* treatment affects T_H17 cells in experimental salt-sensitive hypertension and analysed intestinal and splenic lymphocytes by flow cytometry. Compared to NSD, a HSD led to a significant increase in $CD4^+RORγt^+$ T_H17 cell frequencies in siLPL, which was significantly reduced by *L. murinus* treatment (Fig. 4c). In addition, flow cytometry analysis of siLPL, cLPL and splenic lymphocytes revealed a significant reduction in T_H17 cell frequencies by *L. murinus* treatment compared to HSD feeding alone (Fig. 4d–f). The effect of HSD and concomitant *L. murinus* treatment on effector T cells was again mostly specific to T_H17 cells, as a similar pattern was not observed for T_H1 markers. Except in the siLPL, HSD and *L. murinus* treatment did not alter the expression of the T_H1 cytokine IFNγ (Extended Data Fig. 9 h–j). In addition, the frequencies

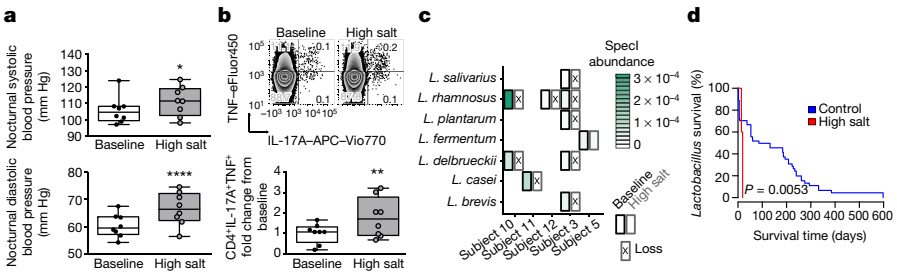

Figure 5 | High-salt challenge affects blood pressure, T_H17 cells and *Lactobacillus* species in healthy humans. a, Mean nocturnal systolic and diastolic blood pressures. **b**, IL-17A$^+$TNF$^+$ (TNF is also known as TNFα) cells in CD4$^+$ enriched peripheral blood mononuclear cells (one representative subject is shown) in $n = 8$ males at baseline and after challenge. Box plots show median and IQR, whiskers are minimum and maximum values. *$P < 0.05$; **$P < 0.01$; ****$P < 0.0001$; paired one-tailed *t*-test (**a**) and Wilcoxon signed-rank test (**b**). **c**, Loss of *Lactobacillus* species after high-salt challenge. Subjects positive for *Lactobacillus* at baseline are shown. Split cells show abundance at baseline (left) and after high salt intake (right), crosses indicate not detected (loss). **d**, Kaplan–Meier curves comparing the persistence of *Lactobacillus* after high salt intake compared to control cohorts (log-rank test).

of regulatory CD4$^+$CD25$^+$ Foxp3$^+$ T (T_{reg}) cells were not significantly affected by either the HSD or concomitant *L. murinus* treatment in intestinal and splenic tissues (data not shown). Thus, *L. murinus* prevents HSD-induced generation of T_H17 cells and consequently ameliorates salt-sensitive hypertension.

Salt challenge in healthy humans

To corroborate our findings in humans, we conducted an exploratory pilot study in healthy male volunteers, where participants were subjected to an increased salt intake for 14 days. Participants received 6 g sodium chloride per day (corresponding to 2.36 g Na^+ per day) using slow-release NaCl tablets in addition to their accustomed diets. According to dietary records, salt intake from foods and drinks was similar between baseline and on day 14 of high salt intake. During the high-salt challenge, the total salt intake was 13.8 ± 2.6 g per day (Extended Data Fig. 10a). We monitored ambulatory blood pressure at baseline and after salt challenge in a subgroup of 8 participants. To standardize blood pressure measurements and exclude physical activity or stress-driven alterations during daytime[30] unrelated to salt sensitivity, we monitored nocturnal blood pressure during bed rest. Compared to baseline, the high-salt challenge significantly increased mean nocturnal systolic and diastolic blood pressure (Fig. 5a). Because the HSD increased the number of T_H17 cells in mice, we analysed T_H17 cells in human blood before and after the high-salt challenge. Analysis of peripheral blood lymphocytes using flow cytometry revealed a significant increase in CD4$^+$IL-17A$^+$TNF$^+$ T_H17 cells (Fig. 5b).

To investigate the effect of a high-salt challenge on the human gut microbiome, we analysed the abundance of *Lactobacillus* species in faecal samples before and after the high-salt challenge. To achieve a more detailed taxonomic resolution, a full shotgun metagenomic analysis was performed (see Supplementary Information). *Lactobacillus* is not a dominant member of the human faeces. In a previously published control dataset[31,32], 41.3% of subjects were positive for any *Lactobacillus* species. In our present study, similarly, 5 out of 12 (41.7%) subjects were positive for at least one gut *Lactobacillus* species at baseline (Fig. 5c). Overall, we detected seven different gut *Lactobacillus* species at baseline (Fig. 5c, species assignment using the species identification (SpecI)[33] metagenomic analysis framework). After the high-salt challenge, nine out of ten *Lactobacillus* populations that were initially present could no longer be detected in the respective study subjects, suggesting a loss of *Lactobacillus* species (Supplementary Information and Extended Data Fig. 10b–d for cross-validation). To test whether this is expected for the human gut over time, we reanalysed 121 published Illumina-sequenced healthy gut metagenomes[31,32] with time course information. A Kaplan–Meier survival analysis on all *Lactobacillus* populations revealed a significantly decreased survival (defined here as continued detectability) rate of *Lactobacillus* gut populations with a HSD (Fig. 5d). Compared to non-*Lactobacillus* species, *Lactobacillus* strains were lost significantly faster with a HSD, reflecting the effect of high salt on a taxon with an intrinsically low resilience (Supplementary Information and Extended Data Fig. 10e, f). Furthermore, we observed that several study subjects had gained at least one new *Lactobacillus* species by day 14 that had not been detected at baseline (Extended Data Fig. 10g–i). We speculate that this is the consequence of ingested *Lactobacillus*-containing foods, since study participants were not subjected to dietary restrictions. Therefore, a high-salt challenge induces an increase in blood pressure and T_H17 cells in healthy subjects, alongside reducing survival of intestinal *Lactobacillus* species in subjects with *Lactobacillus* at baseline.

Discussion

Here we show the effect of increased salt consumption on intestinal bacteria in mice and humans and expand the existing knowledge on the effects of this nutrient. Several intestinal bacteria were affected by high salt; particularly, *Lactobacillus* spp. were suppressed. In addition, faecal metabolites levels, particularly bacterial tryptophan metabolites, responded to HSD in mice. Such effects may contribute to salt-induced T_H17 cell responses and salt-sensitive conditions. Because *L. murinus* produces ILA, we speculate that its salt-induced decrease with reduced ILA generation could be responsible for an increased T_H17 cell response. Importantly, the experimental approaches in mice demonstrate that *L. murinus* supplementation blunts HSD-induced T_H17 activation and ameliorates salt-sensitive hypertension and actively induced EAE *in vivo*. However, actively induced EAE differs from spontaneous disease models[14]. It is therefore currently unclear whether high salt effects can be generalized beyond the actively induced model and to multiple sclerosis. These limitations may also extend to the recent controversy regarding the more general effects of a HSD on neuroinflammation[34,35]. However, in the actively induced EAE and hypertension models used here, and in humans, high salt increased T_H17 cell frequencies.

Lactobacillus metabolites are known to affect host physiology[24,36] and ameliorate actively induced EAE[28]. Other tryptophan metabolites have been shown to reduce blood pressure[37]. Our data in mice suggest that *L. murinus* may substantially influence the abundance of faecal tryptophan metabolites, although we cannot exclude the possibility that other strains (for example, *Bifidobacterium* spp.) may be producers of similar importance. Additionally, we demonstrated that ILA inhibited mouse polarization of T_H17 cells *in vitro*, a finding that needs to be addressed in more detail *in vivo*. These results highlight the microbiome as a salt-sensitive compartment but do not speak against a more direct effect of high salt on host cells. Earlier investigations have shown that the ionic microenvironment directly affects various immune cells[38–41]. Salt intake also has profound actions on hormonal systems, such as the renin–angiotensin–aldosterone axis.

Our pilot study in humans is limited in power and needs to be validated in a larger cohort. Considering this limitation, it suggests that even a moderate salt challenge may affect the persistence of intestinal

Lactobacillus strains and other bacteria, along with an increase in pro-inflammatory T_H17 cells and salt-sensitive blood pressure changes. Interestingly, newborn infants have the greatest abundance of *Lactobacillus* species, which decreases over time[42,43]. Compared to microbiomes from indigenous populations, abundance of *Lactobacillus* strains in 'Western' gut microbiomes is low[44]. Salt ingestion that already starts at a young age may partially have contributed to the relative loss of *Lactobacillus* strains from Western microbiomes and thereby may have role in the development of hypertension and autoimmunity.

Finally, the development of microbiota-targeted therapies is an intriguing new avenue for many diseases. Nevertheless, changes in microbiome composition or function must first be carefully shown to contribute to any disease. Our experimental data in mice suggest that the gut microbiota might serve as a potential target to counteract salt-sensitive conditions. The identification of *Lactobacillus* as a 'natural inhibitor' of high salt-induced T_H17 cells in mice could serve as a basis for the development of novel prevention and treatment strategies. It is up to randomized controlled trials in humans with diseases to test this hypothesis. Moreover, any future dietary salt intervention trial should thus consider monitoring the microbiome to expand on our observations.

Online Content Methods, along with any additional Extended Data display items and Source Data, are available in the online version of the paper; references unique to these sections appear only in the online paper.

Received 26 July 2016; accepted 10 October 2017.
Published online 15 November 2017.

1. Manzel, A. *et al.* Role of "Western diet" in inflammatory autoimmune diseases. *Curr. Allergy Asthma Rep.* **14,** 404 (2014).
2. O'Donnell, M. *et al.* Urinary sodium and potassium excretion, mortality, and cardiovascular events. *N. Engl. J. Med.* **371,** 612–623 (2014).
3. Weber, M. A. *et al.* Clinical practice guidelines for the management of hypertension in the community: a statement by the American Society of Hypertension and the International Society of Hypertension. *J. Hypertens.* **32,** 3–15 (2014).
4. Taylor, J. 2013. ESH/ESC guidelines for the management of arterial hypertension. *Eur. Heart J.* **34,** 2108–2109 (2013).
5. Mozaffarian, D. *et al.* Global sodium consumption and death from cardiovascular causes. *N. Engl. J. Med.* **371,** 624–634 (2014).
6. Coffman, T. M. Under pressure: the search for the essential mechanisms of hypertension. *Nat. Med.* **17,** 1402–1409 (2011).
7. Wenzel, U. *et al.* Immune mechanisms in arterial hypertension. *J. Am. Soc. Nephrol.* **27,** 677–686 (2016).
8. Guzik, T. J. *et al.* Role of the T cell in the genesis of angiotensin II-induced hypertension and vascular dysfunction. *J. Exp. Med.* **204,** 2449–2460 (2007).
9. Madhur, M. S. *et al.* Interleukin 17 promotes angiotensin II-induced hypertension and vascular dysfunction. *Hypertension* **55,** 500–507 (2010).
10. Norlander, A. E. *et al.* Interleukin-17A regulates renal sodium transporters and renal injury in angiotensin II-induced hypertension. *Hypertension* **68,** 167–174 (2016).
11. Kleinewietfeld, M. *et al.* Sodium chloride drives autoimmune disease by the induction of pathogenic T_H17 cells. *Nature* **496,** 518–522 (2013).
12. Wu, C. *et al.* Induction of pathogenic T_H17 cells by inducible salt-sensing kinase SGK1. *Nature* **496,** 513–517 (2013).
13. Miossec, P., Korn, T. & Kuchroo, V. K. Interleukin-17 and type 17 helper T cells. *N. Engl. J. Med.* **361,** 888–898 (2009).
14. Bettelli, E. Building different mouse models for human MS. *Ann. NY Acad. Sci.* **1103,** 11–18 (2007).
15. David, L. A. *et al.* Diet rapidly and reproducibly alters the human gut microbiome. *Nature* **505,** 559–563 (2014).
16. Turnbaugh, P. J. *et al.* An obesity-associated gut microbiome with increased capacity for energy harvest. *Nature* **444,** 1027–1031 (2006).
17. Honda, K. & Littman, D. R. The microbiota in adaptive immune homeostasis and disease. *Nature* **535,** 75–84 (2016).
18. Ivanov, I. I. *et al.* Induction of intestinal Th17 cells by segmented filamentous bacteria. *Cell* **139,** 485–498 (2009).
19. Cole, J. R. *et al.* Ribosomal Database Project: data and tools for high throughput rRNA analysis. *Nucleic Acids Res.* **42,** D633–D642 (2013).
20. Lozupone, C. & Knight, R. UniFrac: a new phylogenetic method for comparing microbial communities. *Appl. Environ. Microbiol.* **71,** 8228–8235 (2005).
21. Sun, Z. *et al.* Expanding the biotechnology potential of lactobacilli through comparative genomics of 213 strains and associated genera. *Nat. Commun.* **6,** 8322 (2015).
22. Wannemuehler, M. J., Overstreet, A. M., Ward, D. V. & Phillips, G. J. Draft genome sequences of the altered Schaedler flora, a defined bacterial community from gnotobiotic mice. *Genome Announc.* **2,** e00287–e14 (2014).
23. Li, J. *et al.* An integrated catalog of reference genes in the human gut microbiome. *Nat. Biotechnol.* **32,** 834–841 (2014).
24. Zelante, T. *et al.* Tryptophan catabolites from microbiota engage aryl hydrocarbon receptor and balance mucosal reactivity via interleukin-22. *Immunity* **39,** 372–385 (2013).
25. Jangi, S. *et al.* Alterations of the human gut microbiome in multiple sclerosis. *Nat. Commun.* **7,** 12015 (2016).
26. Berer, K. *et al.* Commensal microbiota and myelin autoantigen cooperate to trigger autoimmune demyelination. *Nature* **479,** 538–541 (2011).
27. Haghikia, A. *et al.* Dietary fatty acids directly impact central nervous system autoimmunity via the small intestine. *Immunity* **43,** 817–829 (2015).
28. Rothhammer, V. *et al.* Type I interferons and microbial metabolites of tryptophan modulate astrocyte activity and central nervous system inflammation via the aryl hydrocarbon receptor. *Nat. Med.* **22,** 586–597 (2016).
29. Khalesi, S., Sun, J., Buys, N. & Jayasinghe, R. Effect of probiotics on blood pressure: a systematic review and meta-analysis of randomized, controlled trials. *Hypertension* **64,** 897–903 (2014).
30. Hansen, T. W. *et al.* Predictive role of the nighttime blood pressure. *Hypertension* **57,** 3–10 (2011).
31. Forslund, K. *et al.* Country-specific antibiotic use practices impact the human gut resistome. *Genome Res.* **23,** 1163–1169 (2013).
32. Voigt, A. Y. *et al.* Temporal and technical variability of human gut metagenomes. *Genome Biol.* **16,** 73 (2015).
33. Mende, D. R., Sunagawa, S., Zeller, G. & Bork, P. Accurate and universal delineation of prokaryotic species. *Nat. Methods* **10,** 881–884 (2013).
34. Farez, M. F., Fiol, M. P., Gaitán, M. I., Quintana, F. J. & Correale, J. Sodium intake is associated with increased disease activity in multiple sclerosis. *J. Neurol. Neurosurg. Psychiatry* **86,** 26–31 (2015).
35. Fitzgerald, K. C. *et al.* Sodium intake and multiple sclerosis activity and progression in BENEFIT. *Ann. Neurol.* **82,** 20–29 (2017).
36. Lamas, B. *et al.* CARD9 impacts colitis by altering gut microbiota metabolism of tryptophan into aryl hydrocarbon receptor ligands. *Nat. Med.* **22,** 598–605 (2016).
37. Wang, Y. *et al.* Kynurenine is an endothelium-derived relaxing factor produced during inflammation. *Nat. Med.* **16,** 279–285 (2010).
38. Binger, K. J. *et al.* High salt reduces the activation of IL-4- and IL-13-stimulated macrophages. *J. Clin. Invest.* **125,** 4223–4238 (2015).
39. Eil, R. *et al.* Ionic immune suppression within the tumour microenvironment limits T cell effector function. *Nature* **537,** 539–543 (2016).
40. Hernandez, A. L. *et al.* Sodium chloride inhibits the suppressive function of $FOXP3^+$ regulatory T cells. *J. Clin. Invest.* **125,** 4212–4222 (2015).
41. Jantsch, J. *et al.* Cutaneous Na^+ storage strengthens the antimicrobial barrier function of the skin and boosts macrophage-driven host defense. *Cell Metab.* **21,** 493–501 (2015).
42. Cox, L. M. *et al.* Altering the intestinal microbiota during a critical developmental window has lasting metabolic consequences. *Cell* **158,** 705–721 (2014).
43. Tamburini, S., Shen, N., Wu, H. C. & Clemente, J. C. The microbiome in early life: implications for health outcomes. *Nat. Med.* **22,** 713–722 (2016).
44. Martínez, I. *et al.* The gut microbiota of rural Papua New Guineans: composition, diversity patterns, and ecological processes. *Cell Reports* **11,** 527–538 (2015).

Supplementary Information is available in the online version of the paper.

Acknowledgements We thank G. N'diaye, I. Kamer, S. Seubert, P. Voss, J. Anders, C. Schmidt, A. Geuzens, R. Hercog and S. Kandels-Lewis for assistance; and J. J. Mullins and F. C. Luft for their support. This study was funded by grants from the German Centre for Cardiovascular Research (DZHK; BER 1.1 VD), the Center for Microbiome Informatics and Therapeutics, and the MetaCardis consortium. D.N.M., J.J. and M.G. were supported by the German Research Foundation (DFG). R.A.L. holds an endowed professorship supported by Novartis Pharma. M.K. was supported by the European Research Council (ERC) under the European Union's Horizon 2020 research and innovation program (640116), by a SALK-grant from the government of Flanders, Belgium and by an Odysseus-grant of the Research Foundation Flanders (FWO), Belgium. *L. reuteri* was provided by L. Romani.

Author Contributions N.W. led and conceived the project, designed and performed most experiments, analysed and interpreted the data. M.G.M., S.W.O. and S.M.K. performed 16S sequencing and data analysis. S.H., D.T., M.Ba. and C.W. performed animal experiments and analysed data. H.B., S.H., A.B., D.A.G. and B.F.C.-R. performed and analysed flow cytometry. L.Mai., S.M.K., V.S., P.N. and R.G.G. performed bacterial growth experiments. O.V. and C.F. performed metabolite analysis with input from A.B. and M.G.M. L.Mar., F.H.K. and L.K. performed 16S qPCR. N.R. performed sodium analyses. K.F. performed metagenomic analyses with contributions from P.I.C. and S.S. M.Bo., R.D. and A.M. conducted the clinical study. A.K. performed statistical analyses. M.G., A.T., J.M.T., S.K., P.B. and J.J. supervised the experiments and analyses. D.N.M., E.J.A., M.K. and R.A.L. conceived the project, supervised the experiments and interpreted the data. N.W. and D.N.M. wrote the manuscript with key editing by E.J.A., R.A.L., M.K. and K.F. and further input from all authors.

Author Information Reprints and permissions information is available at www.nature.com/reprints. The authors declare no competing financial interests. Readers are welcome to comment on the online version of the paper. Publisher's note: Springer Nature remains neutral with regard to jurisdictional claims in published maps and institutional affiliations. Correspondence and requests for materials should be addressed to D.N.M. (dominik.mueller@mdc-berlin.de) or E.J.A. (ejalm@mit.edu).

Reviewer Information *Nature* thanks T. Coffman, D. A. Relman, H. Wekerle and the other anonymous reviewer(s) for their contribution to the peer review of this work.

METHODS

Animal ethics. All animal experiments were conducted in accordance with institutional, state and federal guidelines and with permission of the local animal ethics committees (Landesamt für Gesundheit und Soziales Berlin, Germany; Regierung Unterfranken, Würzburg, Germany; Ethical Committee for Animal Experiments, Hasselt University, Belgium). Male mice were maintained on a 12:12 h day:night cycle with constant access to food and water.

Mouse high salt feeding and faeces collection. All normal salt (NSD, E15430-047) and high salt (HSD, E15431-34) purified diets used for mouse experiments were purchased from Ssniff (Soest, Germany). Diets were gamma-irradiated (25 kGy) and identical in composition except for NaCl content (NSD: 0.5% NaCl, HSD: 4% NaCl). Drinking water for HSD animals was supplemented with 1% NaCl.

For faecal microbiome analyses, male FVB/N mice aged 12 weeks were purchased from Charles River and accustomed to NSD. Control animals remained on the NSD ($n=8$), others were switched to HSD ($n=12$) for 14 days. A subgroup was switched back to NSD for another 14 days ($n=8$). Body weight and food intake were monitored. To avoid cage effects, mice were housed individually. Fresh faecal pellets were collected directly from the anal orifices, immediately flash-frozen in liquid nitrogen and stored at −80 °C for later analyses.

DNA extraction from mouse faeces and 16S sequencing. DNA was extracted from a single faecal pellet from each mouse using the Power Soil kit (MO BIO Laboratories). The protocol was modified from the manufacturer's instructions to include proteinase K treatment to further lyse the cells. After addition of proteinase K (final concentration 5 mg ml^{-1}) samples were incubated at 65 °C for 10 min and a further 10 min at 95 °C. Plates were inverted to mix during both incubations. The V4 region of the 16S rRNA gene was amplified with 515F and 806R primers[45] using a two-step PCR library preparation as previously described[46]. An Illumina MiSeq was run for 250 cycles to produce paired-end reads.

16S rDNA data processing. The raw sequences were de-multiplexed, allowing at most 2 mismatches in the barcode before discarding a sequence. Primers sequences were removed, allowing at most 2 mismatches in the primer sequence before discarding a sequence. Forward and reverse reads were merged by comparing alignments with lengths of 253 ± 5 nucleotides. The alignment with the fewest mismatches was used unless the number of mismatches was greater than 2, in which case the read pair was discarded. Merged reads were filtered for quality by removing reads with more than 2.0 expected errors[47]. Each unique sequence was assigned a taxonomy using the ribosomal database project[48], truncating the taxonomy to the highest taxonomic level with at least 80% support. Sequences that were assigned the same taxonomy were then placed in the same OTU. *De novo* OTUs were also called using usearch[49].

16S rDNA data analysis. For most analyses, three samples were excluded because their read counts were low (<1,000 counts). The MDS ordination and PERMANOVA test were computed using the vegan package[50] in R. The phylogenetic tree was generated from a single medoid sequence from each OTU. Medoid sequences were selected by aligning all the sequences in each OTU with PyNAST[51], computing a distance matrix with Clustal Omega[52], and selecting the medoid sequence. Aligned sequences with at least 10 reads in their corresponding OTU were assembled into a tree with FastTree v.2.0 (ref. 53) and visualized with the ape package[54] in R. The AdaBoost classifier[55] was run with 10^7 estimators using the scikit-learn module[56] in Python. The random forest classifier[57] was run with 10^6 estimators also using the scikit-learn module in Python.

Faecal metabolite analysis. An extraction mixture of methanol:chloroform:water (MCW; 5:2:1 v-v:v) (methanol LC–MS-grade, chloroform, Reagent Plus 99,8% Sigma-Aldrich) with cinnamic acid (2 μg ml^{-1}, Sigma-Aldrich) as internal standard was added to the sample. Samples were dissolved in MCW (1 ml per 60 mg of sample) using the tissue lyser (Precellys 24 lysis and homogenization, Bertin Technologies), samples were cooled on ice between the shaking cycles. Samples were shaken at 1,000 r.p.m. and 4 °C for 60 min. After addition of ice-cold water (half of the MCW volume), samples were shaken at 1,000 r.p.m. and 4 °C for 10 min. Samples were centrifuged for 10 min at 14,000 r.p.m. to separate the polar (top), lipid (bottom) and interface (tissue debris) layers. the polar phase containing metabolites was dried under vacuum for 12 h.

Samples were derivatized as follows: the dried extracts were dissolved in 20 μl of methoxyamine hydrochloride solution (Sigma-Aldrich; 40 mg ml^{-1} in pyridine (Roth)) and incubated for 90 min at 30 °C shaken at 1,000 r.p.m. followed by the addition of 40 μl of *N*-methyl-*N*-[trimethylsilyl]trifluoroacetamide (MSTFA; Machery-Nagel) and incubation at 37 °C for 45 min agitated at 1,000 r.p.m. The extracts were centrifuged for 10 min at 14,000 r.p.m., and aliquots of 30 μl were transferred into glass vials (Chromacol) for GC–MS measurements. Metabolite analyses were performed with a Pegasus IV mass spectrometer (LECO) as described previously[58]. The GC–MS chromatograms were pre-processed with the ChromaTOF software (LECO). Calculation of retention index, mass spectra identification and metabolite quantification were performed using the in-house Maui-SILVIA software tool[59].

Measured values from 66 metabolites were obtained. Because a paired analysis (metabolites at NSD baseline versus metabolites after HSD) was performed, absence of a given value made the exclusion of the corresponding second value necessary. This was in only 33 out of 1,056 cases (3.1%). A small pseudocount value (0.001) was added to all metabolite values and data were $\log_{10}$ transformed. Data from each metabolite were normalized by subtracting the minimum and dividing by the maximum value across all eight mice. A PCA was performed using the PCA module in the scikit-learn package of Python. The heat map was prepared with the clustermap function of the Seaborn package.

Measurement of tryptophan metabolites. Faecal pellets derived from mice were processed as previously described[24]. Chemicals used were purchased from Sigma-Aldrich and were liquid chromatography (LC)–MS grade. Pellets were diluted in 0.2 M acetate buffer (pH 4.2) at 300 μl per 10 mg faeces and shaken with 1.5 ml methyl *tert*-buthyl ether (MTBE) on a shaker at room temperature at 1,400 r.p.m. for 10 min in the presence of ceramic beads (2.8 mm Precellys Ceramic Beads, Peqlab). Samples were afterwards centrifuged at 4 °C at 9,000*g*. From the organic phase, 1 ml was transferred into a new Eppendorf vial and samples were concentrated using an Eppendorf Concentrator 5301. Concentrated samples were dissolved in 200 ml acetonitrile:H_2O 1:4 v-v containing 0.2% formic acid and stored at −20 °C for further analysis.

LC–MS/MS analysis was performed using an Agilent 1290 Infinity II UPLC system coupled to an Agilent 6495 Triple Quad mass spectrometer equipped with an iFunnel ESI ion source operated in positive mode (Agilent Technologies). The UPLC column used was an Agilent Eclipse plus (100 mm × 2.1 mm, 1.8 μm). Chromatography was performed under gradient conditions using mobile phase A (0.1% formic acid in water) and B (0.1% formic acid in methanol). The gradient was started at 5% methanol, increased to 95% after 10 min with a constant flow rate of 0.3 ml min^{-1} during a total run time of 17 min. The column temperature was set to 30 °C. The injection volume was 1 μl. Drying gas was adjusted at 130 °C per 17 l min^{-1}, sheath gas at 400 °C per 11 l min^{-1}. Capillary and nozzle voltage were optimized at 3,500 V and 800 V, respectively. Analytes were monitored in the multiple reaction monitoring mode. The optimal transitions, collision energies and cell accelerator voltages for each compound were determined as follows: ILA: 206 → 118 *m/z*, CE: 24 V, CAV: 1 V; IAld 146 → 118 *m/z*, CE: 13 V, CAV: 5 V; IAA 176 → 130 *m/z*, CE: 17 V, CAV: 1 V. Calibration curves for the quantification of individual metabolites were established based on the changes in the relative peak area in response to different target compound concentration. Linearity was $r^2 > 0.99$ over a range of 0.05–300 ng ml^{-1} for any compound.

Isolation of *L. murinus*. Faecal samples from healthy male NSD-fed FVB/N mice were dissolved and diluted at a 1:10 dilution in anaerobic phosphate-buffered saline (PBS) (pH 7.6) containing L-cysteine HCl at 0.1% in a Coy Anaerobic Chamber (5% H_2, 20% CO_2, 75% N_2). Samples were diluted tenfold and each dilution spread on LAMVAB agar[60]. Plates were incubated at 37 °C under anaerobic conditions and examined for growth at 24 h. Individual colonies growing at the highest dilution were picked into LAMVAB medium and grown for an additional 16 h. Liquid cultures were stored in 15% DMSO. For identification of isolates, DNA was extracted by adding 5 μl liquid culture to 20 μl sterile distilled water and storing at 4 °C overnight; 2 μl of this extract was amplified with Phusion HF polymerase in a 20-μl reaction using universal 16S primers 27F (5′-AGAGTTTGATCMTGGCTCAG-3′) and 1492R (5′-TACGGYTACCTTGTTACGACTT-3′). PCR products were purified using Agencourt AMPure XP and submitted with the 27F primer for Sanger sequencing. An isolate for which the full-length 16S sequence shared 100% identity with the V4–V5 region of the *Lactobacillus* species identified in the 16S library was selected for further study. Frozen stocks of *L. murinus* (in PBS with 25% glycerol) were prepared, stored at −80 °C and used for gavage of salt-sensitive and EAE mice.

Salt tolerance of *L. murinus* and selected gut commensals. Frozen stocks of *L. murinus* were streaked onto MRS agar and incubated at 37 °C under aerobic conditions for 24 h. Single colonies were picked into MRS medium and grown until mid-log phase ($OD_{600}=0.4$–0.6), at which time liquid cultures were diluted 1:100 into MRS medium containing NaCl in the range of 0–2 OsM. In separate experiments, *E. coli* and *L. murinus* were picked into LB (*E. coli*) or MRS (*L. murinus*) medium. The Na^+ concentration of growth medium was determined using atomic absorption spectrometry or calculated. The OD_{600} of cultures was measured after an additional 12–16 hours of growth. For comparison of the salt tolerance of phylogenetically distinct gut commensals, *C. difficile* ATCC 700057, *A. muciniphila* DSM 26127 and *P. excrementihominis* DSM 21040 were cultured under the same conditions. Frozen stocks of each strain, along with *L. murinus*, were streaked onto Brucella Blood Agar with vitamin K and haematin, and grown at 37 °C in a Coy Anaerobic Chamber for 24 h. Individual colonies were transferred into liquid Gifu anaerobic medium supplemented with 0.25% porcine gastric mucin

(Sigma-Aldrich) and grown until mid-log phase, at which time they were diluted 1:100 into MGAM containing NaCl with concentrations of Na^+ ranging from 0.08 to 1.8 M. OD_{600} of cultures was measured after 48 h of growth (to compensate for the slow growth rates of some of the strains).

***In vitro* growth of human-associated *Lactobacillus* isolates.** Human-associated *Lactobacillus* isolates were obtained from the German Culture Collection (DSMZ): *L. salivarius* (DSM-no. 20555), *L. ruminis* (DSM-no. 20403), *L. delbrueckii* subsp. Delbrueckii (DSM-no. 20074), *L. fermentum* (DSM-no. 20052). *L. acidophilus* NCFM, *L. paracasei* (ATCC SD5275). *Lactobacillus* strains were grown anaerobically in a gas chamber (Coy Laboratory Products; 12% CO_2, 2.5–5% H_2 and 83–85.5% N_2) in Gifu Anaerobic Medium Broth (MGAM) at 37 °C. Overnight cultures were diluted to an initial OD of 0.01 and growth was assessed in the presence of increasing concentrations of NaCl by monitoring the absorbance at 578 nm using an Eon (Biotek) microplate spectrophotometer at 30-min intervals after 30 s of shaking. AUCs were calculated using the trapezoidal rule and normalized to the AUC calculated for growth in MGAM without addition of NaCl.

Germ-free mice and *L. murinus* monocolonization. C57BL/6J male mice were bred under germ-free conditions and kept in a 12-h light cycle and fed sterile NSD (E15430-047, Ssniff) *ad libitum*. For monocolonization, mice were gavaged with 200 µl of *L. murinus* stock solution (10^7 CFU ml^{-1}, as described above) and further maintained under sterile conditions for two weeks. Faecal pellets were collected under sterile conditions and immediately frozen in liquid nitrogen, or cultured in liquid thioglycolate medium (bioMerieux), incubated for seven days, streaked on sheep blood agar plates (Oxoid, 24 h) and further analysed for species identification using MALDI–TOF (analysed by GIMmbH) as described previously[61].

Salt-sensitive hypertension in mice. To induce salt-sensitive hypertension, the L-NAME/salt mouse model was used as described previously[62]. This non-surgical intervention closely recapitulates salt-sensitive hypertension common in humans[62]. In brief, NSD-fed male FVB/N mice, aged 10–12 weeks, received pretreatment with L-NAME (0.5 mg ml^{-1}, Sigma-Aldrich) in drinking water for three weeks, followed by a one-week washout period with NSD and normal drinking water. Then, mice were switched to either HSD with oral administration of *L. murinus* (daily gavage of 200 µl 10^7 CFU ml^{-1} *L. murinus* suspension), HSD with oral administration of control solution (daily gavage of 200 µl PBS:glycerol) or NSD for two weeks. For blood pressure measurements, mice were implanted with miniature subcutaneous radiotelemetry devices under anaesthesia (Data Sciences International) before the L-NAME/salt protocol. Thereby, systolic and diastolic blood pressures were recorded continuously at 5-min intervals in freely moving mice. Following hypertension induction with HSD for three weeks, HSD was continued and mice were concomitantly gavaged with 200 µl 10^7 CFU ml^{-1} *L. murinus* in PBS and glycerol daily. *L. reuteri* and *E. coli* Nissle 1917 were used for separate experiments in a similar manner (10^7 CFU ml^{-1} in PBS and glycerol daily).

Mice were euthanized under anaesthesia and spleens and intestines were collected. Single-cell suspensions of the small intestinal (si) and colonic (c) lamina propria lymphoyctes (LPL) were obtained by enzymatic and mechanical dissociation using the Mouse Lamina Propria Dissociation kit (Miltenyi Biotec, Bergisch Gladbach, Germany) according to the manufacturer's protocol. Cell debris was removed using a Percoll (GE Healthcare) density gradient centrifugation as described previously[63]. Splenocyte single-cell suspensions were obtained using 70-µm strainers, followed by erythrocyte lysis and subsequent filtering using a 40-µm mesh. Cells were counted by trypan blue exclusion and labelled for flow cytometry analysis.

Isolated immune cells were either directly stained for surface markers using the respective fluorochrome-conjugated antibodies (30 min in PBS supplemented with EDTA and BSA) or restimulated with 50 ng ml^{-1} phorbol-12-myristate-13-acetate (PMA, Sigma-Aldrich), 750 ng ml^{-1} ionomycin (Sigma-Aldrich) and 0.75 µl ml^{-1} GolgiStop (BD Bioscience) for 4 h at 37 °C and 5% CO_2 in RPMI 1640 medium (Sigma-Aldrich) supplemented with 10% FBS, 1% penicillin–streptomycin. For all measurements, dead cell exclusion was performed using a fixable viability dye for 405 nm (Thermo Fisher). For intracellular staining, cells were permeabilized and fixed using the FoxP3 Staining Buffer kit (eBioscience) and labelled using the respective antibodies. Antibodies used are listed below. Cells were analysed with the BD FACSCanto II flow cytometer and BD FACSDiva software (BD Bioscience). Data analysis was performed with FlowJo v.10 (FlowJo LLC).

Experimental autoimmune EAE. Male C57BL/6J mice (Charles River), aged 10–12 weeks, were either fed a NSD, a HSD (Ssniff, as described above) with oral administration of *L. murinus* or *L. reuteri* (daily gavage of 200 µl 10^7 CFU ml^{-1} suspension) or a HSD with oral administration of solvent (daily gavage of 200 µl PBS:glycerol). EAE was induced as described previously[11]. In brief, mice were anaesthetized and subcutaneously injected with 200 µg MOG_{35-55} and 200 µg CFA. Pertussis toxin (200 ng per mouse) was applied intraperitoneally on days 0 and 2 after immunization. Clinical symptoms were assessed daily according to a five-point scale ranging from 0 (no symptoms) to 5 (moribund)[11]. For disease courses, only mice with clinical symptoms were included.

On day 17 after immunization, mice were euthanized under anaesthesia and CNS tissue was collected, disrupted with a 5-ml glass homogenizer and strained through a 100-µm cell strainer. The CNS cell suspension was resuspended in 6 ml 30% isotonic Percoll (GE Healthcare) for a three-step density gradient. Lymphocytes were collected from the interphases, washed and further analysed by flow cytometry. Spleens were disrupted with a glass homogenizer, filtered through a 100-µm cell strainer and treated with 0.14 M ammonium chloride to lyse erythrocytes. To analyse the early inflammatory response in the small intestine, a subset of mice was euthanized on day 3 after immunization and the small intestine was collected and processed as described above to obtain LPL.

In two additional experimental setups EAE was induced in male germ-free C57BL/6J mice fed gamma-sterilized (50 Gy) NSD or HSD diets. First, germ-free mice were fed with either NSD or HSD (two weeks before immunization and thereafter). Second, germ-free mice were fed a NSD and either monocolonized with SFB (by introduction of faeces from SFB monocolonized mice) or SFB and *L. murinus*. In both experimental subgroups, intestines were collected on day 3 after immunization for flow cytometry analyses.

Single-cell suspensions were analysed by staining for extra- and intracellular markers. Dead cells were excluded by a fixable viability dye eFluor780 (eBioscience), Fc-block was performed using anti-CD16/32 antibody (eBioscience). For intracellular cytokine staining, cells were stimulated with ionomycin (1 µM) and PMA (50 ng ml^{-1}) in the presence of monensin (2 µM) for 4 h. Cells were stained for surface markers with the respective fluorochrome-conjugated antibodies for 30 min and permeabilized using Fixation and Permeabilization Buffer (eBioscience) according to the manufacturer's protocol. Intracellular cytokines were labelled with the respective fluorochrome-conjugated antibodies for 30–45 min. For antibodies used see below. Cells were analysed with the BD FACSCanto II flow cytometer and BD FACSDiva software (BD Bioscience). Data analysis was performed with FlowJo (LLC).

For quantitative real-time PCR, tissue was homogenized in 500 µl peqGOLD TriFast with an Ultra-Turrax for 30 s followed by total RNA isolation with PerfectBind RNA Columns (peqGOLD HP Total RNA Kit, Peqlab). RNA yield was quantified by absorbance measurements at 260 nm and reverse transcribed into cDNA using QuantiTect transcriptase (Qiagen). PCR reactions were performed at a 5-µl scale on a qTower real-time PCR System (Analytic Jena, Germany) in triplicates using Taqman Assays (Thermo Fisher) for *Il17a* (Mm00439618_m1), *Rorc* (Mm01261019_g1) and *Csf2* (Mm01290062_m1). Relative quantification was performed by the $\Delta\Delta C_t$ method, normalizing target gene expression to *Actb* (β-actin; Mm00607939_s1) as housekeeping gene.

Antibodies used for flow cytometry of mouse cells. Anti-CD3ε–FITC and anti-CD3ε–VioBlue (clone 17A2, Miltenyi Biotec), anti-CD4–APC–Vio770 (clone GK1.5, Miltenyi Biotec), anti-CD4–Pacific blue and anti-CD4–FITC (clone RM4-5, BD), anti-CD25–VioBlue and anti-CD25–FITC (clone 7D4, Miltenyi Biotec), anti-FoxP3–PerCP–Cy5.5 (clone FJK-16s, eBioscience), anti-IFNγ–PE–Cy7 and anti-IFNγ–APC (clone XMG1.2, eBioscience), anti-IL-17A–PE (clone eBio17B7, eBioscience) and anti-RORγt–APC (clone REA278, Miltenyi Biotec).

Electrolyte analysis of mouse faeces. Faecal samples from NSD- and HSD-fed mice were collected and stored at −80 °C until further analysis. $n = 7$–9 faeces samples were pooled, weighed and then processed as described previously[64]. In brief, samples were weighted, desiccated, ashed, dissolved and measured for Na^+ concentration by atomic adsorption spectrometry (Model 3100, Perkin Elmer).

Measurement of intestinal transit. Male FVB/N mice were fed a NSD or HSD for 14 days. Mice were administered activated charcoal (0.5 g per 10 ml in 0.5% methylcellulose; 0.1 ml per 10 g body weight by oral gavage). After 20 min, mice were euthanized and the distance travelled by charcoal was measured.

High-salt challenge study in healthy humans. We performed an open-label clinical pilot study to investigate the effect of an increased salt intake on cardiovascular and immunoregulatory functions in healthy men (https://clinicaltrials.gov/ identifier: NCT02509962). The study was conducted at the Experimental and Clinical Research Center Berlin (ECRC), Germany, in accordance with the ethical standards of the institutional review board. The institutional review board of Charité University Medicine Berlin approved the study (EA1/138/15) and written informed consent was obtained from all participants before study entry. Key inclusion criteria were male, age 18–50 years and a body mass index between 18.5 and 29.9 kg m^{-2}. Key exclusion criteria were any cardiovascular, metabolic (diabetes), autoimmune, liver and kidney diseases, alcohol or drug abuse. To increase salt intake, subjects ($n = 12$, included until March 2016, for baseline characteristics see Supplementary Information) received 10 coated tablets daily (three with breakfast, three with lunch and four with dinner) for two weeks, each tablet containing 600 mg sodium chloride in a slow release formulation (Slow Sodium Tablets, HK Pharma Ltd), yielding

an increase of habitual salt intake by 6 g per day. Subjects were asked not to change their dietary habits during the study. Sodium intake from ingested foods and drinks was calculated from dietary records of three consecutive days using OptiDiet Plus software v.5.1.2 (GOE mbH), a professional analysis software that is based on nutritional content of food as provided by the German Nutrient Database[65].

Stool samples were collected at baseline and on day 13 of the high-salt challenge from all 12 subjects. In brief, subjects collected fresh faecal samples using disposable toilet seat covers (Süsse Labortechnik) and plastic vessels with spatula (Sarstedt AG). Closed vessels with faecal samples were immediately frozen in a domestic freezer at –20 °C and subsequently transferred to the study centre on dry ice, where samples were stored at –80 °C until further use.

At baseline and on day 13 of the high-salt challenge, 8 subjects received ambulatory blood pressure monitors (ABPM, Mobil-O-Graph, I.E.M. GmbH) for nocturnal blood pressure monitoring (measurements at bed rest every 30 min, subjects indicated bed rest by pressing the day/night button of the ABPM).

Venous blood was taken at baseline and on day 14 of the HSD for immediate isolation of peripheral blood mononuclear cells.

Metagenomic sequencing of human faecal samples. Samples were processed, extracted and sequenced as previously described[32] with SpecI[33] and mOTU[66] taxonomic abundances estimated using MOCAT[67]. Because *Lactobacillus* has a low abundance in the human gut, to verify results are robust to changes in the bioinformatic protocol, samples were additionally processed using the complementary tool MetaPhlan[68], which uses lineage-specific marker genes as opposed to the universal marker genes informing SpecI and mOTU species quantification, with MetaPhlan species detection results almost identical to mOTU species detection results (Extended Data Fig. 10a, b).

Previously published healthy human gut shotgun metagenomes where multiple samples from the same individual at different time points were available were taken from ref. 32 and from the Human Microbiome Project (2012, processed as described previously[31]). Survival analysis was done using the survival package[69] in R as outlined in ref. 70.

Human blood cell analysis. Peripheral venous blood was obtained from study participants. Peripheral blood mononuclear cells were immediately isolated by density centrifugation using Biocoll (Merck). Subsequently, 10^6 $CD4^+$ enriched cell fractions isolated using the $CD4^+$ T Cell kit (Miltenyi Biotec) were plated onto U-bottom plates and were restimulated for 4 h at 37 °C, 5% CO_2 in a humidified incubator. Restimulation was conducted in a final volume of 200 µl RPMI 1640 (Sigma-Aldrich) supplemented with 10% FBS (Merck), 100 U ml^{-1} penicillin (Sigma-Aldrich), 100 mg ml^{-1} streptomycin (Sigma-Aldrich), 50 ng ml^{-1} PMA (Sigma-Aldrich), 250 ng ml^{-1} ionomycin (Sigma-Aldrich) and 1.3 µl ml^{-1} Golgistop (BD). After restimulation, cells were stained with the Life/Dead Fixable Aqua Dead Cell kit (Thermo Fisher) and monoclonal CD3–PerCP–Vio700 antibody (clone BW264/56, Miltenyi Biotec). Cells were fixed and permeabilized with the Foxp3/Transcription Factor Staining Buffer kit (eBioscience) and labelled using anti-IL-17A–APC–Vio770 (clone CZ8-2361, Miltenyi Biotec) and anti-TNF–eFluor450 (clone Mab11, eBioscience) monoclonal antibodies. Cells were analysed using a FACSCanto II flow cytometer and FACSDiva software (BD). Data analysis was performed with FlowJo (LLC).

Mouse T_H17 cell polarization. Splenic T cells were isolated by magnetic-activated cell sorting using the Pan T cell isolation kit II (Miltenyi Biotec) according to the manufacturer's instructions. Isolated T cells were collected and resuspended in MACS buffer at 3×10^7 cells per ml. For APC-free differentiation, cells were fluorescently stained for 30 min in an antibody cocktail containing anti-CD4–FITC (RM4-5, eBioscience), anti-CD44–PE (IM7, BioLegend), anti-CD62L–APC (MEL-14, eBioscience) and anti-CD25–PE–Cy5 (PC61.5, eBioscience) and subsequently purified by fluorescence-activated cell sorting on MoFlo (Beckman-Coulter). Sorted naive T cells ($CD4^+CD62L^+CD44^{low}CD25^-$) were stimulated by plate-bound anti-CD3 (2 µg ml^{-1}, 145-2C11, BD Pharmingen) and anti-CD28 (2 µg ml^{-1}, 37.51, BD Pharmingen) in the presence of IL-6 (40 ng ml^{-1}) and rhTGFβ1 (2 ng ml^{-1}). To determine the influence of ILA on T_H17 cell differentiation, cells were cultured with vehicle (0.1% ethanol) or 10–500 µM ILA for 96 h under isotonic or hypertonic (+40 mM NaCl) conditions.

DNA extraction from faeces and qPCR of 16S rRNA genes. DNA from stool samples was isolated using QIAamp DNA Stool Mini Kit (Qiagen) according to the manufacturer's instructions. To optimize the representation of the bacterial community structure, a mutanolysin (Sigma-Aldrich) digestion step was included (6 µl of 25 kU ml^{-1} stock per sample)[71]. qPCR on a 7500 Sequence Detector (Applied Biosystems, AB) was used to calculate the number of bacterial 16S rRNA gene copies in the genomic DNA extracted from stool samples. Samples were quantified in 10-µl reactions containing 1× SYBR Green Master Mix (AB), 300 nM of each primer and 4 ng of genomic DNA. Standard curves for quantification consisted of tenfold serial dilutions in the range of 10^8–10^0 copies of the 16S rRNA gene of the *E. coli* (Invitrogen, C404010) or *L. murinus* isolates amplified with primers 27F (5′-GTTTGATCCTGGCTCAG-3′) and 1492R (5′-CGGCTACCTTGTTACGAC-3′)[72]. The total amount of bacterial 16S in stool samples was quantified with universal primers, Univ 337F 5′-ACTCCTACGGGAGGCAGCAGT-3′ and Univ 518R 5′-GTATTACCGCGGCTGCTGGCAC-3′[73]. The total amount of different *Lactobacillus* DNA in stool samples was quantified using the following primers: *L. murinus/animalis*[74], LactoM-F (5′-TCGAACGAAACTTCTTTATCACC-3′) and LactoM-R (5′-CGTTCGCCACTCAACTCTTT-3′); *L. brevis*[75], LbrevF (5′-TGCACTGATTTCAACAATGAAG-3′) and LbrevR (5′-CCAGAAGTG ATAGCCGAAGC-3′); *L. casei/paracasei*[76], LcaseF (5′-GCACCGAGATTCA ACATGG-3′) and LcaseR (5′-GGTTCTTGGATCTATGCGGTATTAG-3′); *L. delbrueckii*[76], LdelbF (5′-GGGTGATTTGTTGGACGCTAG-3′) and LdelbR (5′-GCCGCCTTTCAAACTTGAATC-3′); *L. fermentum*[77], LfermF (5′-GCACC TGATTGATTTTGGTCG-3′) and LactoR (5′-GTCCATTGTGGAAGATTCCC-3′); *L. plantarum*[78] sg-Lpla-F (5′-CTCTGGTATTGATTGGTGCTTGCAT-3′) and sg-Lpla-R (5′-GTTCGCCACTCACTCAAATGTAAA-3′); *L. rhamnosus*[76], LrhamF (5′-TGCTTGCATCTTGATTTAATTTTG-3′) and LactoR (5′-GTCCATTG TGGAAGATTCCC-3′); *L. salivarius*[77], LsalivF (5′-CGAAACTTTCTTA CACCGAATGC-3′) and LactoR (5′-GTCCATTGTGGAAGATTCCC-3′). All measurements were performed in duplicate.

Statistics. Power calculation is a prerequisite for any animal experiment according to the local animal law and was performed using G*Power software v.3.1.9.2. Effect sizes were calculated from previously published experiments. Animals were randomly assigned to the respective body weight-matched groups, probiotic and control treatment were administered without knowledge of the treatment groups. The human pilot study was performed in an unblinded manner. Data analysis was performed by the investigators without knowledge of the treatment groups or treatment phase. All findings shown have been reproduced in at least two independent experiments. Data are presented depending on their scale and distribution with arithmetic mean and standard deviation (mean ± s.e.m.) or median including 25–75% quartiles (25|75). Unless otherwise specified, box plots show median and IQR with whiskers showing minimum and maximum values, bar graphs show mean ± s.e.m. Outliers identified by Grubbs' test were excluded. Normality was assessed using a Kolmogorov–Smirnov test. To compare independent measurements, we used a *t*-test and Mann–Whitney *U*-test, as appropriate. To compare dependent measurements, we used a paired *t*-test or Wilcoxon signed-rank test, as appropriate. To compare more than two groups, we used one-way ANOVA followed by Tukey's post hoc test or Kruskal–Wallis test followed by Dunn's post hoc test, as appropriate. Statistical analysis was performed using GraphPad Prism v.6. *Lactobacillus* survival times are visualized by Kaplan–Meier curves and statistically compared by log-rank test.

To analyse mouse blood pressure telemetry data, we conducted repeated measurement analysis by using linear mixed models. We tested a random intercept versus a random intercept–slope model and selected the best-fit model. Data analysis was performed with R (v.3.1.1 R Foundation, Vienna, Austria) using the packages lme4 and nlme. A P value <0.05 was considered statistically significant.

Code availability. Code used for the 16S rDNA data analysis has been uploaded to a github repository (https://github.com/almlab/analysis-salt-responsive). Software was obtained from publicly available sources; papers describing the software are cited in the text.

Data availability. Raw files of the bacterial V4–V5 16S rRNA data and the *L. murinus* genome have been uploaded to the NCBI Sequence Read Archive as Bioproject PRJNA400793. Raw metagenomic data of the human study are available in the European Nucleotide Archive (ENA, accession number PRJEB22348). Reference datasets for the human metagenome analysis are accessible in the ENA (accession number ERP009422) and from https://www.hmpdacc.org/. Source Data for Figs 1–5 and Extended Data Figs 1, 3–10 are provided with the paper.

45. Caporaso, J. G. *et al.* Ultra-high-throughput microbial community analysis on the Illumina HiSeq and MiSeq platforms. *ISME J.* **6,** 1621–1624 (2012).
46. Preheim, S. P., Perrotta, A. R., Martin-Platero, A. M., Gupta, A. & Alm, E. J. Distribution-based clustering: using ecology to refine the operational taxonomic unit. *Appl. Environ. Microbiol.* **79,** 6593–6603 (2013).
47. Edgar, R. C. & Flyvbjerg, H. Error filtering, pair assembly and error correction for next-generation sequencing reads. *Bioinformatics* **31,** 3476–3482 (2015).
48. Wang, Q., Garrity, G. M., Tiedje, J. M. & Cole, J. R. Naive Bayesian classifier for rapid assignment of rRNA sequences into the new bacterial taxonomy. *Appl. Environ. Microbiol.* **73,** 5261–5267 (2007).
49. Edgar, R. C. Search and clustering orders of magnitude faster than BLAST. *Bioinformatics* **26,** 2460–2461 (2010).
50. Oksanen, J. *et al.* Vegan: Community Ecology Package. R package v.2.3–0 http://CRAN.R-project.org/package=vegan (2015).
51. Caporaso, J. G. *et al.* PyNAST: a flexible tool for aligning sequences to a template alignment. *Bioinformatics* **26,** 266–267 (2010).

52. Sievers, F. *et al.* Fast, scalable generation of high-quality protein multiple sequence alignments using Clustal Omega. *Mol. Syst. Biol.* **7,** 539 (2011).
53. Price, M. N., Dehal, P. S. & Arkin, A. P. FastTree 2—approximately maximum-likelihood trees for large alignments. *PLoS One* **5,** e9490 (2010).
54. Paradis, E., Claude, J. & Strimmer, K. APE: analyses of phylogenetics and evolution in R language. *Bioinformatics* **20,** 289–290 (2004).
55. Freund, Y. & Schapire, R. E. A decision-theoretic generalization of on-line learning and an application to boosting. *J. Comput. Syst. Sci.* **55,** 119–139 (1997).
56. Pedregosa, F. *et al.* Scikit-learn: machine learning in Python. *J. Mach. Learn. Res.* **12,** 2825–2830 (2011).
57. Breiman, L. Random forests. *Mach. Learn.* **45,** 5–32 (2001).
58. Pietzke, M., Zasada, C., Mudrich, S. & Kempa, S. Decoding the dynamics of cellular metabolism and the action of 3-bromopyruvate and 2-deoxyglucose using pulsed stable isotope-resolved metabolomics. *Cancer Metab*. **2,** 9 (2014).
59. Kuich, P. H., Hoffmann, N. & Kempa, S. Maui-VIA: a user-friendly software for visual identification, alignment, correction, and quantification of gas chromatography–mass spectrometry data. *Front. Bioeng. Biotechnol*. **2,** 84 (2015).
60. Hartemink, R., Domenech, V. R. & Rombouts, F. M. LAMVAB—A new selective medium for the isolation of lactobacilli from faeces. *J. Microbiol. Methods* **29,** 77–84 (1997).
61. Gomila, M. *et al.* Genotypic and phenotypic applications for the differentiation and species-level identification of *Achromobacter* for clinical diagnoses. *PLoS One* **9,** e114356 (2014).
62. Itani, H. A. *et al.* CD70 exacerbates blood pressure elevation and renal damage in response to repeated hypertensive stimuli. *Circ. Res.* **118,** 1233–1243 (2016).
63. Atarashi, K. & Honda, K. Analysis of murine lamina propria TH17 cells. Protoc. Exch. http://doi.org/10.1038/nprot.2008.205 (2008).
64. Wiig, H. *et al.* Immune cells control skin lymphatic electrolyte homeostasis and blood pressure. *J. Clin. Invest.* **123,** 2803–2815 (2013).
65. Mähler, A. *et al.* Increased catabolic state in spinocerebellar ataxia type 1 patients. *Cerebellum* **13,** 440–446 (2014).
66. Sunagawa, S. *et al.* Metagenomic species profiling using universal phylogenetic marker genes. *Nat. Methods* **10,** 1196–1199 (2013).
67. Kultima, J. R. *et al.* MOCAT2: a metagenomic assembly, annotation and profiling framework. *Bioinformatics* **32,** 2520–2523 (2016).
68. Segata, N. *et al.* Metagenomic microbial community profiling using unique clade-specific marker genes. *Nat. Methods* **9,** 811–814 (2012).
69. Therneau, T. M. A package for survival analysis in S. v.2.38 https://CRAN.R-project.org/package=survival (2015).
70. Therneau, T. M. & Grambsch, P. M. *Modeling Survival Data: Extending the Cox Model* (Springer, 2000).
71. Yuan, S., Cohen, D. B., Ravel, J., Abdo, Z. & Forney, L. J. Evaluation of methods for the extraction and purification of DNA from the human microbiome. *PLoS One* **7,** e33865 (2012).
72. Caesar, R., Tremaroli, V., Kovatcheva-Datchary, P., Cani, P. D. & Bäckhed, F. Crosstalk between gut microbiota and dietary lipids aggravates WAT inflammation through TLR signaling. *Cell Metab.* **22,** 658–668 (2015).
73. Bergström, A. *et al.* Introducing GUt low-density array (GULDA): a validated approach for qPCR-based intestinal microbial community analysis. *FEMS Microbiol. Lett.* **337,** 38–47 (2012).
74. Bindels, L. B. *et al.* Restoring specific lactobacilli levels decreases inflammation and muscle atrophy markers in an acute leukemia mouse model. *PLoS One* **7,** e37971 (2012).
75. Duniere, L. *et al.* Impact of adding *Saccharomyces* strains on fermentation, aerobic stability, nutritive value, and select lactobacilli populations in corn silage. *J. Anim. Sci*. **93,** 2322–2335 (2015).
76. Byun, R. *et al.* Quantitative analysis of diverse *Lactobacillus* species present in advanced dental caries. *J. Clin. Microbiol.* **42,** 3128–3136 (2004).
77. Cui, Y. *et al.* Different effects of three selected *Lactobacillus* strains in dextran sulfate sodium-induced colitis in BALB/c mice. *PLoS One* **11,** e0148241 (2016).
78. Matsuda, K. *et al.* Establishment of an analytical system for the human fecal microbiota, based on reverse transcription–quantitative PCR targeting of multicopy rRNA molecules. *Appl. Environ. Microbiol.* **75,** 1961–1969 (2009).

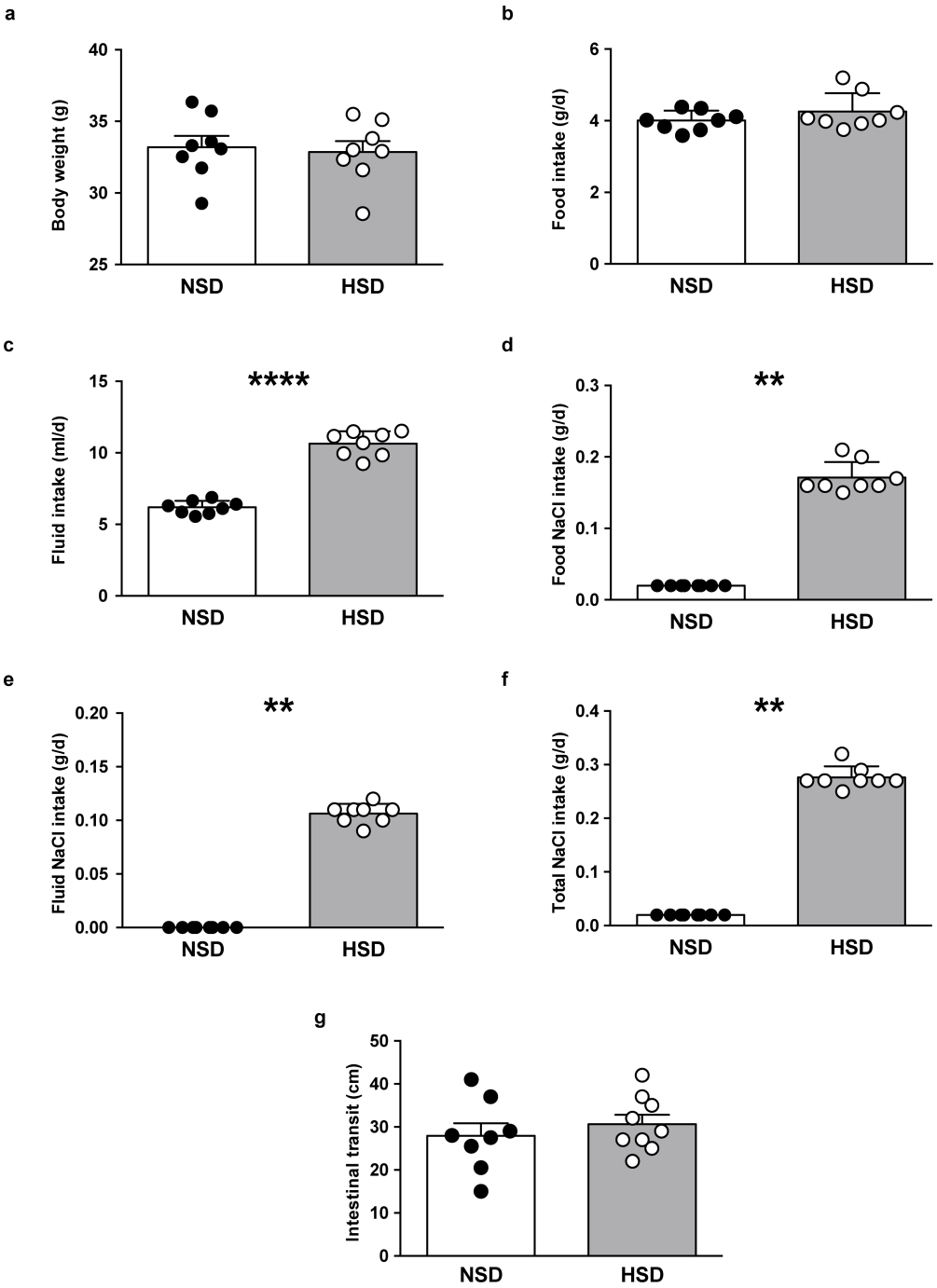

Extended Data Figure 1 | Body weight, food, fluid and sodium chloride (NaCl) intake, and intestinal transit in mice fed a NSD or HSD. **a**–**f**, Body weight (**a**), food intake (**b**), fluid intake (**c**), NaCl intake from the chow (**d**), NaCl intake from the drinking water (**e**) and total NaCl intake (**f**; sum of NaCl intake from chow and drinking water) in mice fed a NSD ($n = 8$) or HSD ($n = 8$). **g**, Measurement of intestinal transit. FVB/N mice were fed a NSD ($n = 8$) or HSD ($n = 9$) for 14 days and administered activated charcoal (0.5 g per 10 ml in 0.5% methylcellulose; 0.1 ml per 10 g body weight by oral gavage). After 20 min, mice were euthanized and the distance travelled by charcoal was measured. Data are mean ± s.e.m., circles represent individual mice. $^{**}P < 0.01$; $^{****}P < 0.001$; paired two-tailed Student's *t*-test (**a**–**c**), one-tailed Wilcoxon matched-pairs signed-rank test (**d**–**f**), unpaired two-tailed Student's *t*-test (**g**).

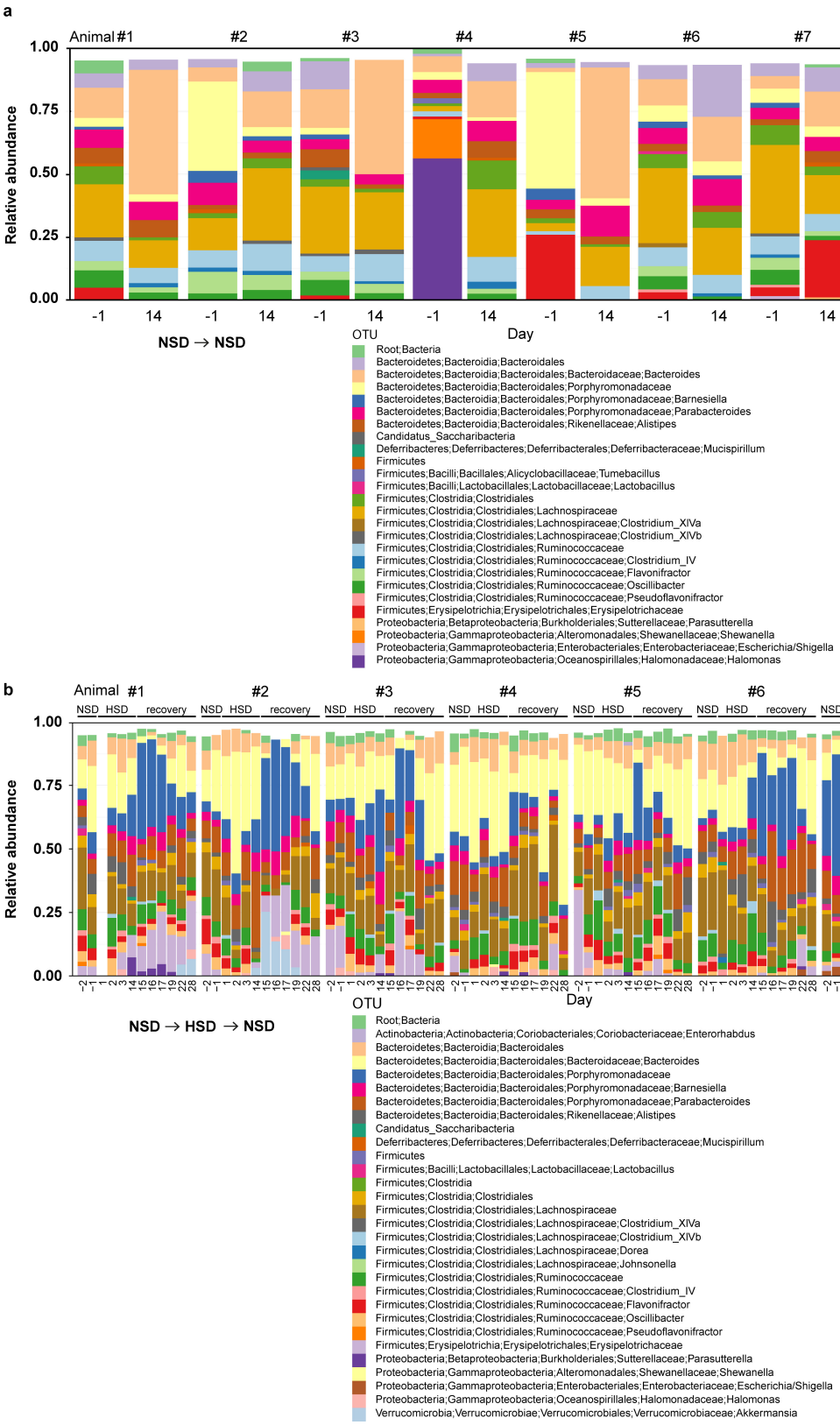

Extended Data Figure 2 | Faecal microbiome profiles of mice kept on a NSD or HSD over time. Taxonomic bar charts showing relative abundance of ribosomal database project-based OTUs on indicated days. **a**, Mice remaining on a NSD for 14 days served as NSD controls. Baseline NSD day −1 and NSD day 14 are shown. **b**, Separate mice were switched from NSD (days −2 and −1) to HSD for 14 days, and were finally re-exposed to NSD for another 14 days (recovery). For time course analyses, faecal samples from baseline NSD days (−1 and −2), early (days 1–3) and late (day 14) HSD days and NSD recovery days (days 15–17, 19, 22, 28) are shown. $n = 8$ mice per group.

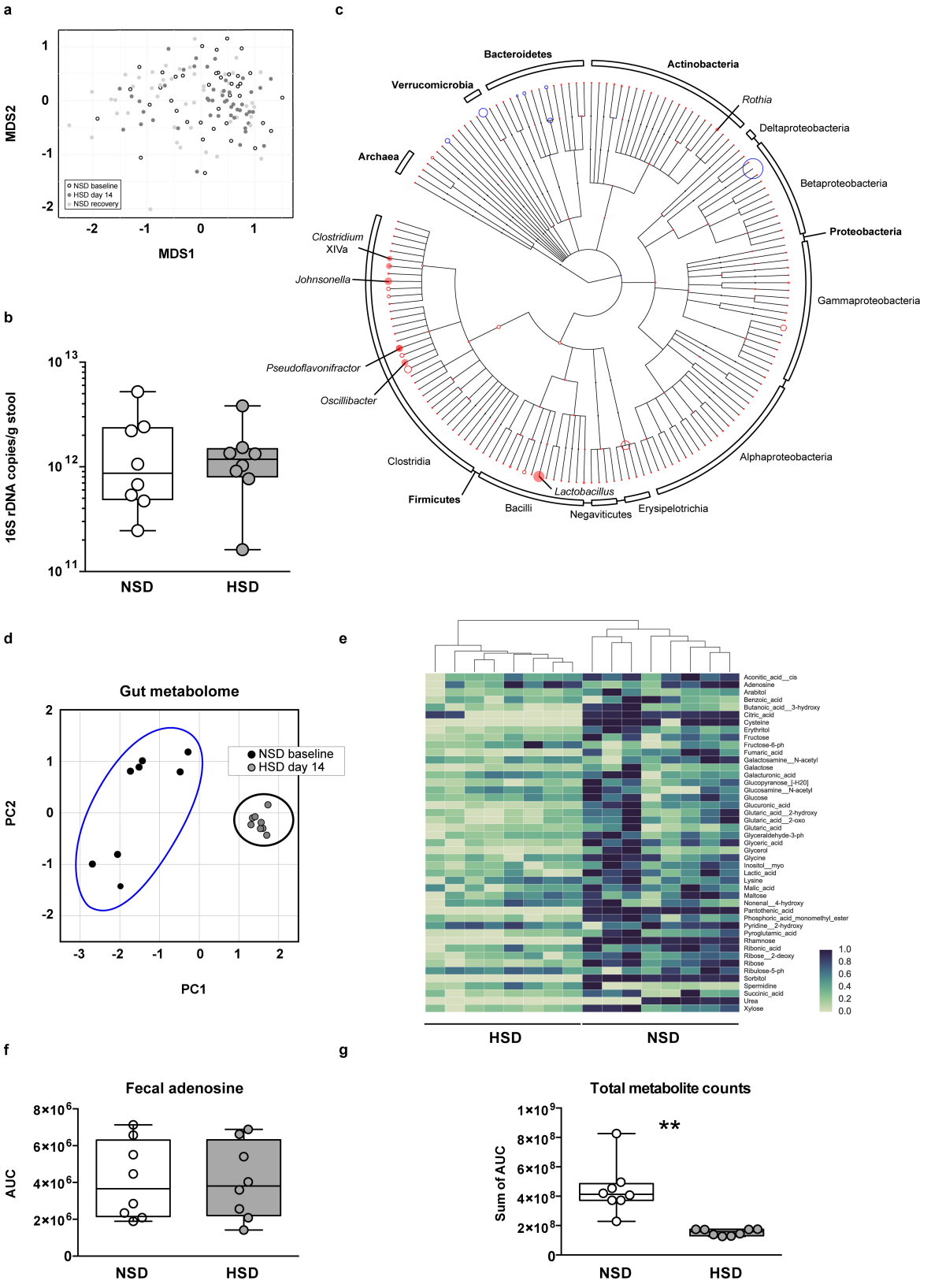

Extended Data Figure 3 | See next page for caption.

Extended Data Figure 3 | HSD alters the faecal microbiome and the faecal metabolite profile. a, Mouse 16S rDNA faecal microbiome samples do not separate by diet in a MDS ordination (white, NSD samples; black, HSD samples; grey, recovery on NSD). **b**, qPCR of DNA extracted from faecal samples of mice fed a NSD or HSD using universal 16S rDNA primers ($n = 8$ faecal samples per group from independent mice, indicated by circles; two-tailed Wilcoxon matched-pairs signed-rank test). **c**, Phylogenetic tree showing changes in microbiome composition caused by HSD. OTUs present in samples from day 14 are indicated by coloured circles (red indicates reduction in HSD samples; blue indicates enrichment). The radius of each circle indicates a median log-fold difference in relative abundance between the two diets. Filled circles mark statistically significant differences (two-tailed Student's *t*-test, Benjamini–Hochberg correction, $P < 0.05$). **d**–**g**, High dietary salt strongly influences the faecal metabolite profile. Male FVB/N mice ($n = 8$) were fed a NSD and then switched to HSD. Metabolites were extracted from faecal pellets taken from mice on a NSD (day −3) and HSD (day 13), and analysed by GC–MS. **d**, HSD samples are clearly distinguishable from NSD samples in a principal component analysis for faecal metabolites. **e**, Faecal metabolites clearly cluster by treatment. The majority of faecal metabolites are reduced by HSD. Hierarchically clustered heat map, metabolites shown in alphabetical order. Metabolites were normalized by subtracting the minimum and dividing by the maximum value across all mice. **f**, Faecal levels of the nucleoside adenosine were similar in both diets, suggesting that the change in metabolites is not due to a decrease in overall bacterial biomass. **g**, HSD leads to a reduction in total metabolite peak intensities in faecal samples. $^{**}P < 0.01$; two-tailed paired Student's *t*-test (**f**, **g**).

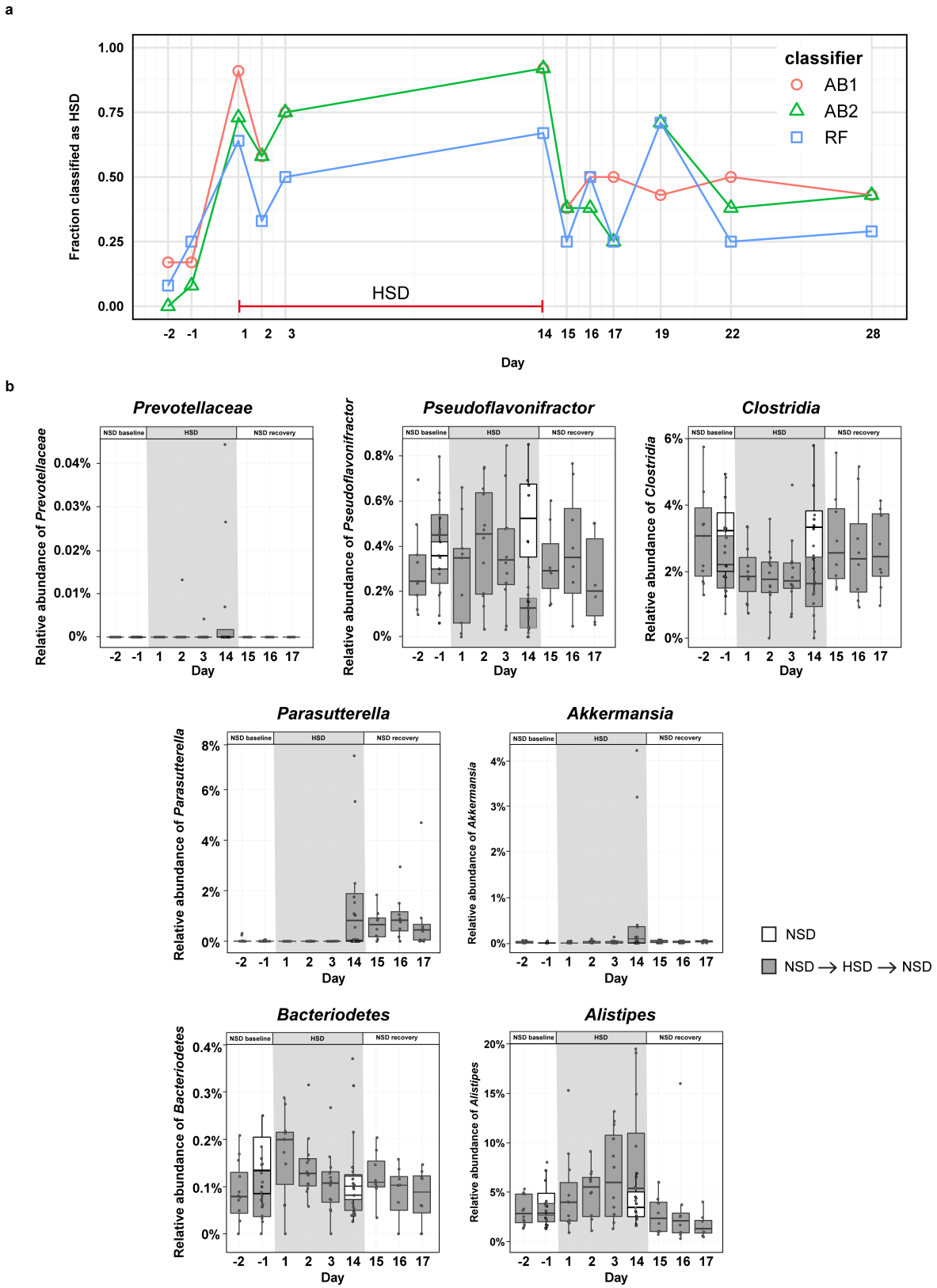

Extended Data Figure 4 | Accuracy of AdaBoost and random forest classifiers. a, AdaBoost and random forest classifiers (trained on samples from days −2, −1 and 14) were used to predict the classification of all samples from HSD mice. The fraction of samples from each time point that the classifiers predicted as belonging to animals currently on a HSD is shown. The two runs of the random forest produced the same fractions, so only one line is shown for the two random forest classifiers. **b**, Time series for the remaining 7 OTUs important to the classifier. NSD and HSD phases are indicated by white and grey backgrounds. Mice ($n = 12$) were switched from NSD to HSD and back to NSD (subgroup of $n = 8$). Other control mice ($n = 8$) that remaind on NSD are shown in white. Box plots show median, IQR with whiskers of 1.5× IQR, circles represent samples from independent mice.

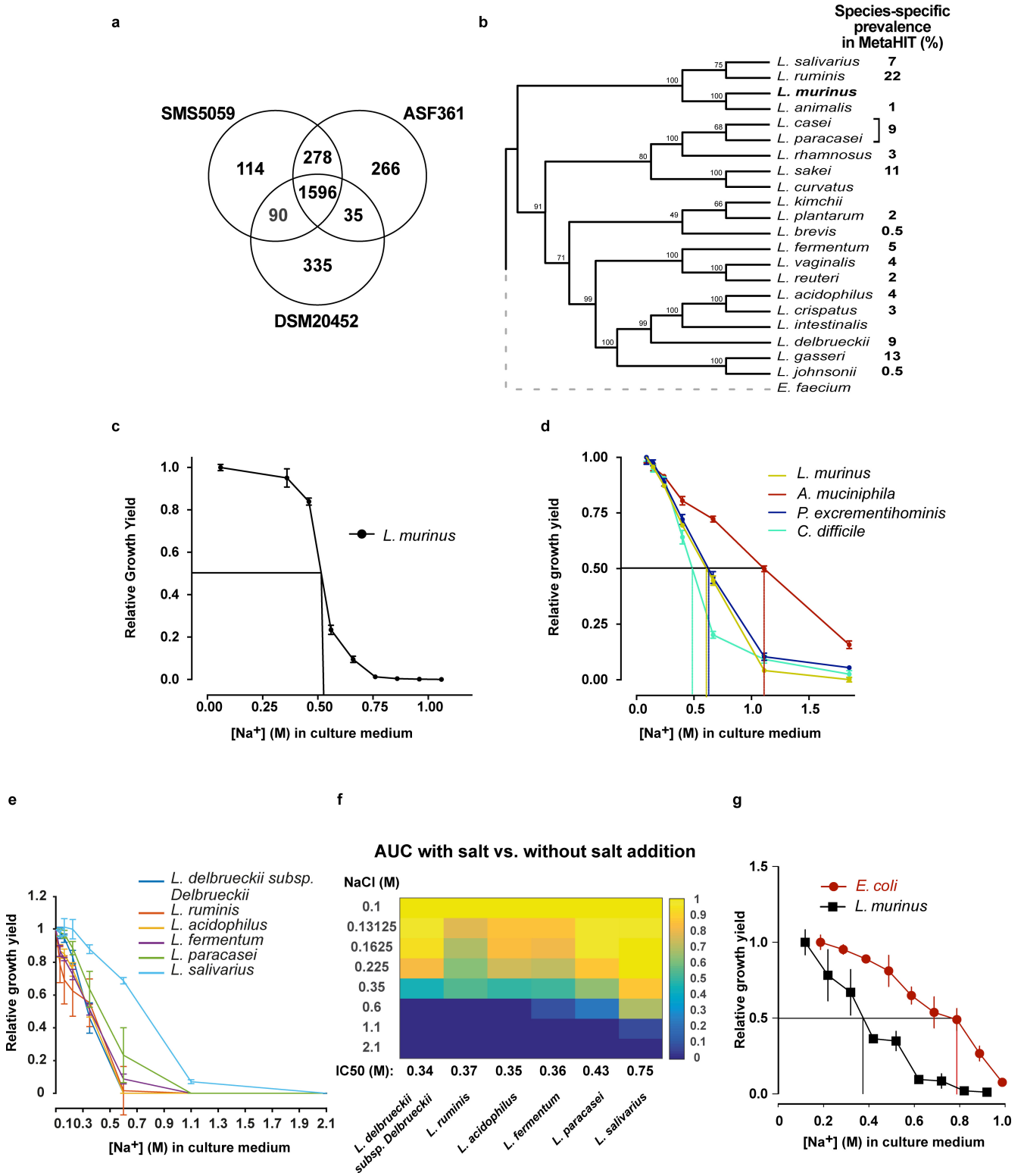

Extended Data Figure 5 | *L. murinus* genome and *in vitro* growth of *Lactobacilli*. **a**, Venn diagram of the coding sequences present in the *L. murinus* and two other isolates with available with full genome sequences. **b**, Bootstrapped phylogenetic tree of full-length 16S rDNA from a variety of *Lactobacillus* species resident in rodent or human guts. Prevalence of the respective species in the MetaHIT cohort is shown. *L. murinus* strains are absent from the MetaHIT cohort. **c**, Growth yield (OD_{600}) of *L. murinus* measured at increasing concentrations of NaCl. Aerobic endpoint measurements of liquid *L. murinus* cultures in MRS medium and increasing NaCl concentrations relative to growth in MRS without the addition of NaCl. $n = 5$ independent experiments. **d**, Anaerobic growth yield of *L. murinus*, *A. muciniphila*, *P. excrementihominis* and *C. difficile* grown at 37 °C for 48 h in MGAM liquid medium. Growth at each salt concentration is normalized to growth at 0.086 M Na^+. The respective IC_{50} is indicated. $n = 3$ technical replicates across two experiments. **e**, Anaerobic growth of selected human *Lactobacillus* species in MGAM medium with increasing NaCl concentrations. Relative growth yield is calculated based on AUCs by comparing to growth in MGAM without the addition of NaCl. $n = 3$ independent experiments with three technical replicates. **f**, Heat map showing data as in **e**. The respective IC_{50} is shown in the bottom row. **g**, Growth yield of *E. coli* and *L. murinus*, grown at 37 °C for 12–16 h in LB (*E. coli*) or MRS broth (*L. murinus*). $n = 4$ technical replicates from two independent experiments. Data are mean ± s.e.m.

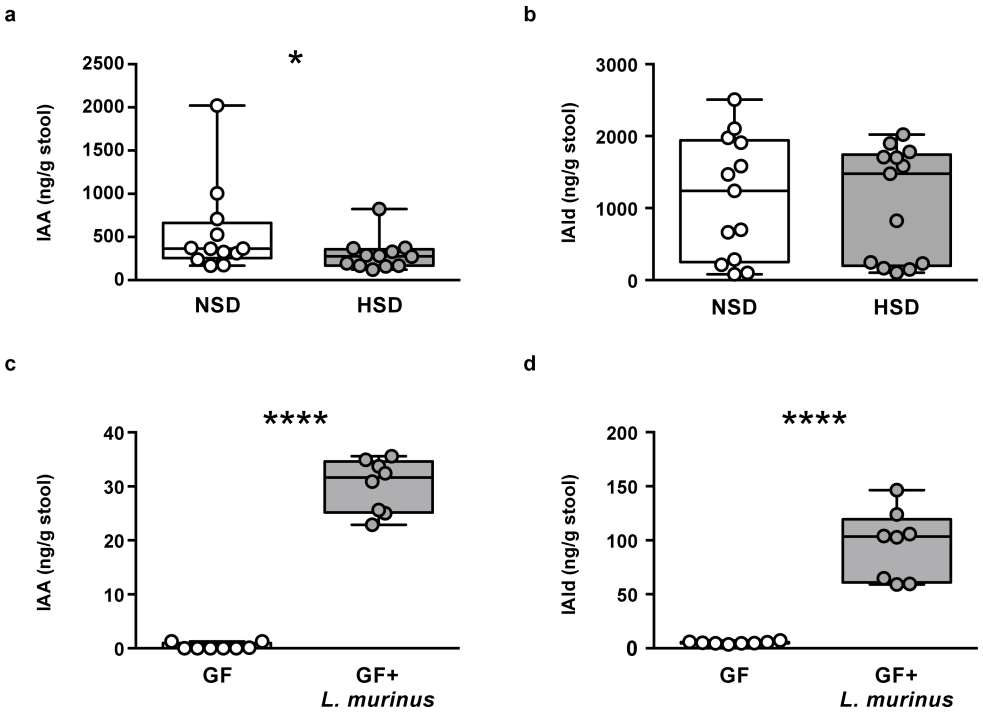

Extended Data Figure 6 | Indole metabolites in mouse faecal samples. **a**, **b**, Effect of HSD on faecal IAA (**a**) and IAld (**b**) content in FVB/N mice fed a NSD or HSD ($n = 12$ per group in **a**; $n = 13$ per group in **b**). **c**, **d**, Germ-free (GF) mice monocolonized with *L. murinus* showed increased faecal IAA and IAld content ($n = 8$ per group). $^{*}P < 0.05$; $^{****}P < 0.0001$; one-tailed Wilcoxon matched-pairs signed-rank test (**a**, **b**), one-tailed Mann–Whitney *U*-test (**c**), unpaired one-tailed Student's *t*-test (**d**). *n* represents the number of independent mice.

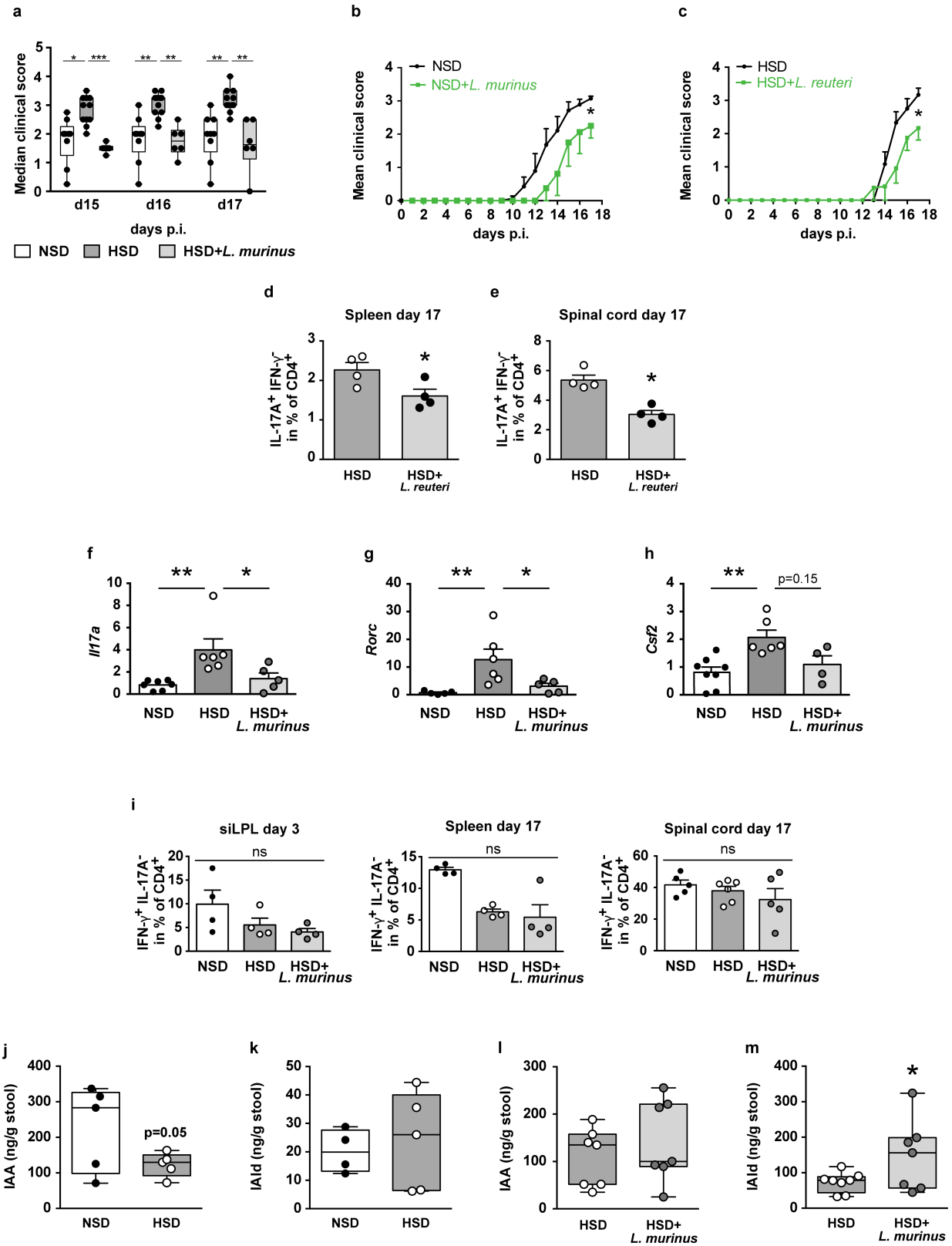

Extended Data Figure 7 | See next page for caption.

Extended Data Figure 7 | The effect of *Lactobacillus* species on actively induced EAE. a, Median cumulative clinical EAE scores at day 15, 16 and 17 post immunization (p.i.) of NSD ($n = 9$), HSD ($n = 11$) and HSD mice treated with *L. murinus* ($n = 6$) starting at the day of immunization. **b**, Clinical course of $MOG_{35–55}$ EAE in NSD mice (black circles, $n = 7$) and NSD mice treated with *L. murinus* (green squares, $n = 4$). **c**, Clinical course of $MOG_{35–55}$ EAE in HSD mice (black circles) and HSD mice treated with *L. reuteri* (green squares, $n = 6$ independent mice per group). **d**, **e**, Quantification of $CD4^+IL\text{-}17A^+IFN\gamma^-$ cells on day 17 of EAE in the spleen (**d**) and spinal cord (**e**). $n = 4$ independent mice per group. **f–h**, Spinal cords on day 17 of EAE were analysed by RT–qPCR for relative expression of *Il17a* (**f**; $n = 7$ for NSD, $n = 6$ for HSD and $n = 5$ for HSD with *L. murinus*), *Rorc* (**g**; $n = 5$ for NSD, $n = 6$ for HSD and $n = 5$ for HSD with *L. murinus*) and *Csf2* (**h**; $n = 8$ for NSD, $n = 6$ for HSD and $n = 4$ for HSD with *L. murinus*). **i**, Quantification of IFNγ-producing T_H1 cells of siLPL on day 3 of EAE ($n = 4$ per group) and quantification of IFNγ-producing T_H1 cells in spleen ($n = 4$ per group) and spinal cord on day 17 of EAE ($n = 5$ for NSD, $n = 6$ for HSD and $n = 5$ for HSD with *L. murinus*). **j–m**, Faecal indole metabolites were determined in $MOG_{35–55}$ EAE mice by LC–MS/MS analysis. Effect of HSD on faecal IAA (**j**) and IAld (**k**) content on day 10 after immunization ($n = 5$ per group (**j**), $n = 4$ for NSD and $n = 5$ for HSD (**k**)). Faecal IAA (**l**) and IAld (**m**) content in $MOG_{35–55}$ EAE mice fed a HSD with or without concomitant *L. murinus* treatment on day 10 after immunization ($n = 7$ per group (**l**), $n = 8$ for HSD and $n = 7$ for HSD with *L. murinus* for (**m**)). Box plots show median and IQR, whiskers are minimum and maximum values (**a**, **j–m**), data are mean ± s.e.m. **b–i**). $^*P < 0.05$, $^{**}P < 0.01$, $^{***}P < 0.001$; ns, not significant; Kruskal–Wallis test followed by Dunn's multiple comparisons test (**a**), two-tailed Mann–Whitney *U*-test (**b**, **c**), one-tailed Mann–Whitney *U* test (**d**, **e**), one-way ANOVA followed by Tukey's post hoc test (**f–h**), one-way ANOVA (**i**), unpaired one-tailed Student's *t*-test (**j**, **l**, **m**), one-tailed Wilcoxon matched-pairs signed-rank test (**k**). *n* represents the number of independent mice per group, indicated by circles.

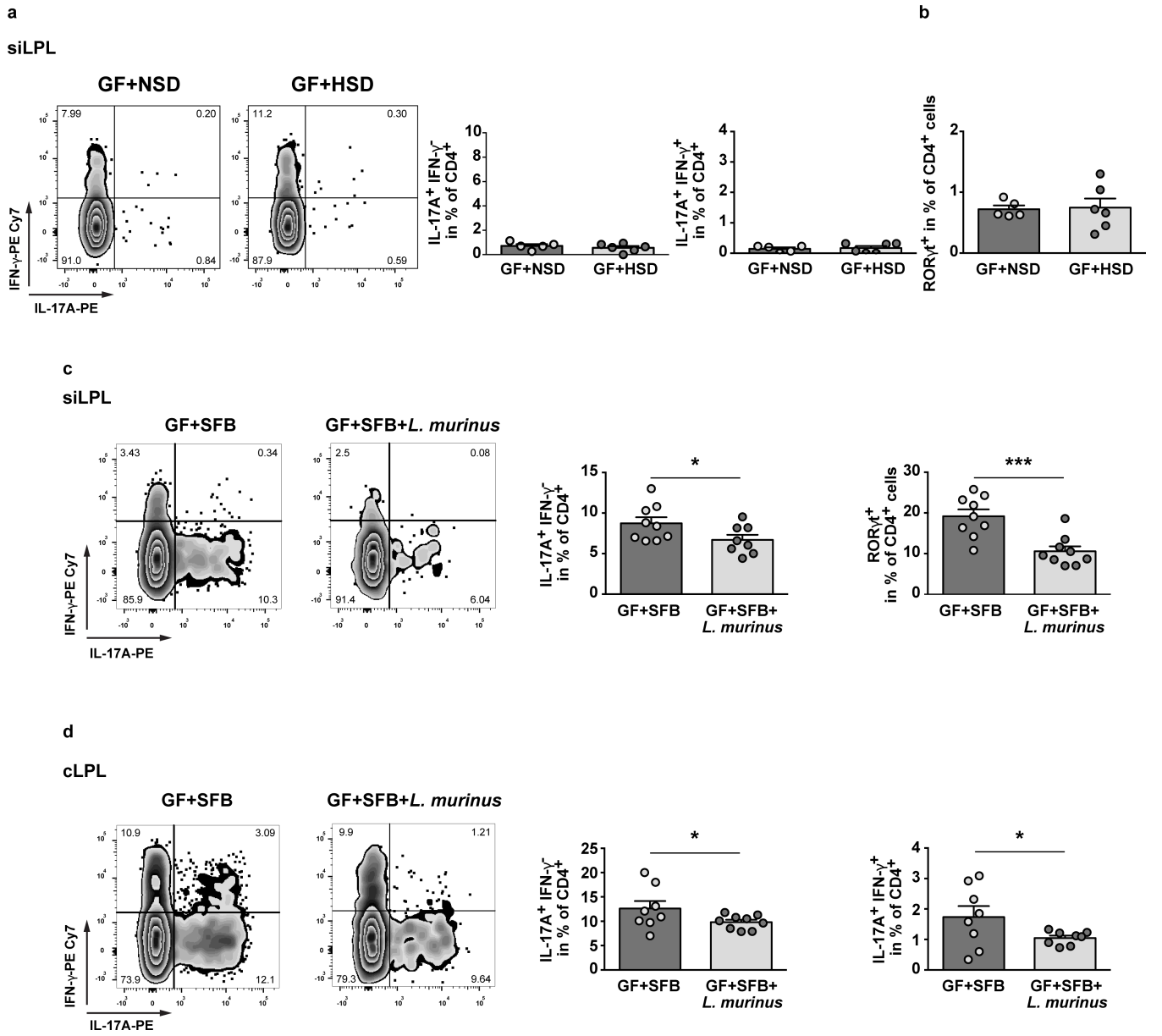

Extended Data Figure 8 | Actively induced EAE in gnotobiotic mice. **a, b**, HSD fails to induce intestinal T_H17 cells in germ-free $MOG_{35–55}$ EAE mice ($n = 5$ for GF + NSD and $n = 6$ for GF + HSD). **a**, Analysis of IL-17A and IFNγ in $CD4^+$ siLPL isolated from NSD or HSD-fed $MOG_{35–55}$-immunized germ-free mice (day 3 after immunization). Representative flow cytometry plots (left) show one mouse per group. Quantifications show frequencies of $CD4^+IL\text{-}17A^+IFN\gamma^-$ (middle) and $CD4^+IL\text{-}17A^+IFN\gamma^+$ (right) cells. **b**, Quantification of $CD4^+ROR\gamma t^+$ frequencies in siLPL. **c**, **d**, *L. murinus* reduces small intestinal (siLPL) and colonic (cLPL) lamina propria T_H17 cells in EAE mice colonized with SFB. $MOG_{35–55}$ EAE was induced in germ-free mice monocolonized with SFB (GF + SFB) and germ-free mice colonized with SFB and *L. murinus* (GF + SFB + *L. murinus*). LPL were isolated on day 3 after immunization. **c**, Left, representative flow cytometry plots demonstrating IL-17A and IFNγ expression in $CD4^+$ siLPL (one mouse per group). Middle, quantification of $CD4^+IL\text{-}17A^+IFN\gamma^-$ siLPL ($n = 9$ for GF + SFB, $n = 8$ for GF + SFB + *L. murinus*). Right, quantification of $CD4^+ROR\gamma t^+$ siLPL ($n = 9$ mice per group). **d**, Left, representative flow cytometry plots (one mouse per group) depicting IL-17A and IFNγ expression in $CD4^+$ cLPL. Middle and right, quantification of $CD4^+IL\text{-}17A^+IFN\gamma^-$ ($n = 8$ for GF + SFB, $n = 9$ for GF + SFB + *L. murinus*) and $CD4^+IL\text{-}17A^+IFN\gamma^+$ cLPL ($n = 8$ per group). Data are mean ± s.e.m., circles represent independent mice. $^*P < 0.05$; $^{***}P < 0.001$; unpaired one-tailed Student's *t*-test (**a**–**d**).

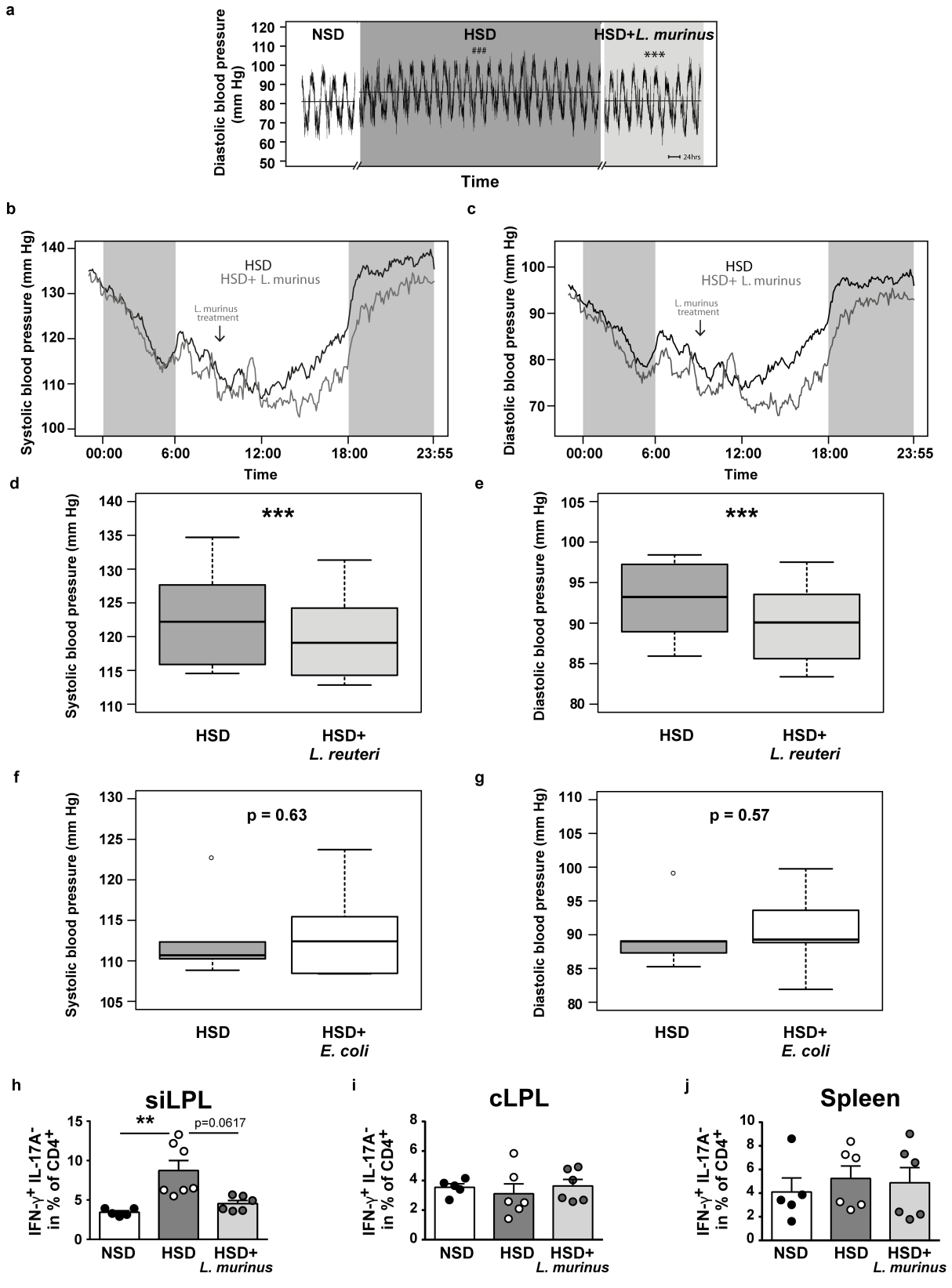

Extended Data Figure 9 | See next page for caption.

Extended Data Figure 9 | Treatment with *L. murinus* or *L. reuteri* ameliorates salt-sensitive hypertension. a, Mean diastolic pressures over time in response to HSD and HSD with concomitant *L. murinus* treatment in $n = 7$ FVB/N mice. Scale bar indicates 24 h. Horizontal line indicates the mean across all values of the respective phase. **b**, **c**, Mean systolic (**b**) and diastolic (**c**) blood pressures in mice ($n = 7$) fed a HSD (black curve) and HSD with concomitant *L. murinus* treatment at circadian scale. Arrows indicate the time of *L. murinus* gavage. **d**, **e**, Box plots (median, IQR, whiskers 1.5× IQR) show systolic (**d**) and diastolic (**e**) blood pressures recorded continuously in FVB/N mice fed a HSD and a HSD with concomitant *L. reuteri* treatment. These mice ($n = 9$) were fed a HSD for 10 days before concomitant *L. reuteri* treatment for another 7 days. $^{***}P < 0.001$ versus HSD using a linear mixed model. **f**, **g**, Box plots (median, IQR, whiskers 1.5× IQR) show systolic (**f**) and diastolic (**g**) blood pressures in mice ($n = 5$) fed a HSD and a HSD with concomitant *E. coli* Nissle 1917 treatment for three days, respectively. Statistics using linear mixed model. **h**–**j**, Quantification of $CD4^{+}IL\text{-}17A^{-}IFN\gamma^{+}$ lymphocytes in siLPL (**h**; $n = 5$ for NSD, $n = 7$ for HSD, $n = 6$ for HSD + *L. murinus*) and cLPL and spleen, respectively (**i**, **j**, $n = 5$ for NSD, $n = 6$ for HSD, $n = 6$ for HSD + *L. murinus*). Data are mean ± s.e.m., circles represent independent mice. $^{*}P < 0.05$; Kruskal–Wallis and Dunn's post hoc test (**h**), one-way ANOVA (**i**, **j**).

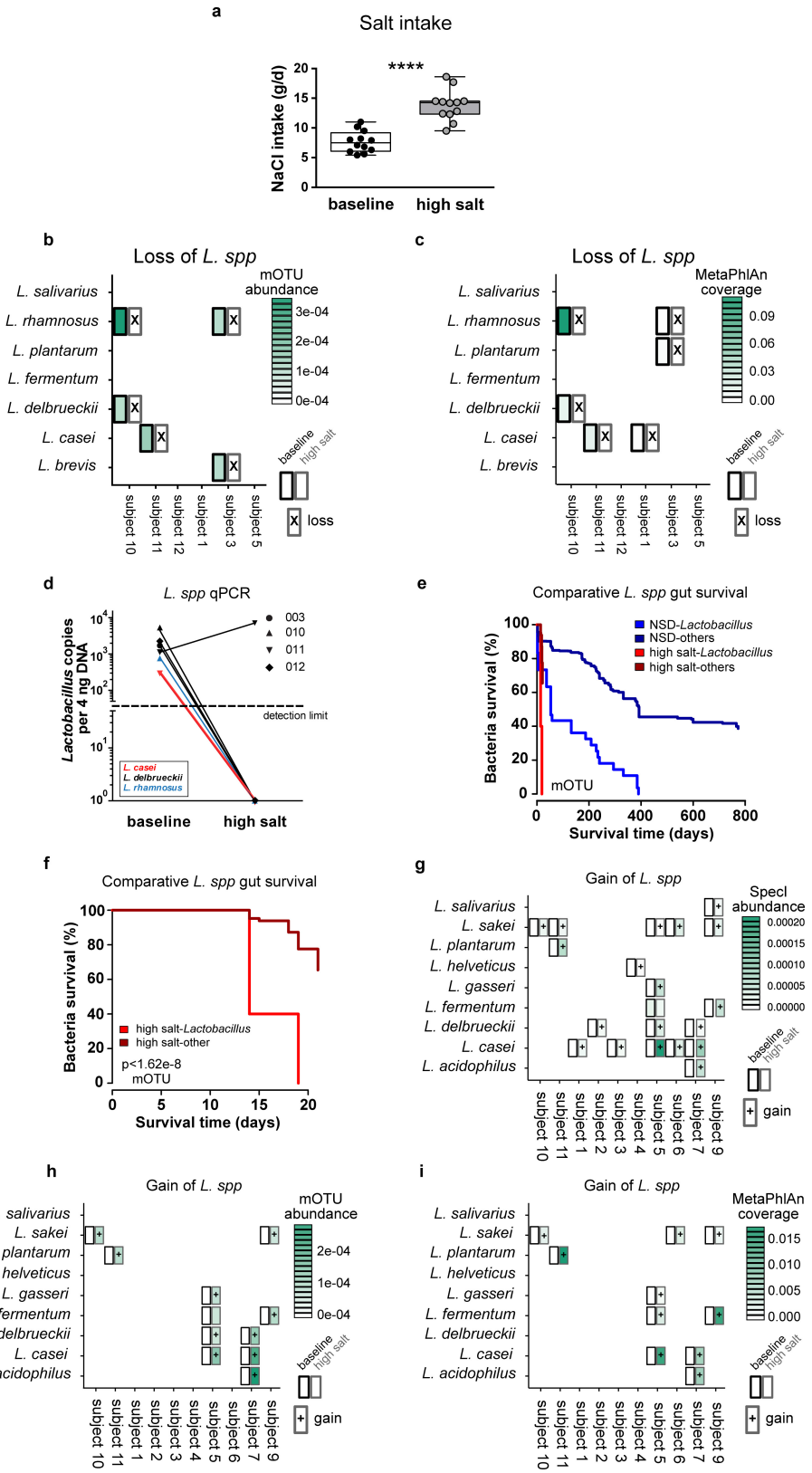

Extended Data Figure 10 | See next page for caption.

Extended Data Figure 10 | High-salt challenge in healthy human subjects. a, Total salt intake according to dietary records ($n = 12$, paired one-tailed *t*-test). **b**, **c**, Metagenome analysis shows loss of *Lactobacillus* gut populations during human high-salt challenge. All subjects (*x* axis) for which gut *Lactobacilli* were detected are shown at baseline and all species detected (*y* axis) using the mOTU (**b**) or MetaPhlAn framework (**c**) for bacterial species identification are shown. Heat map cells show abundance of mOTU (insert counts as fraction of sample total) or average coverage (reads per position) for MetaPhlAn of the *Lactobacillus* species at baseline (left part of cells, black border) and after high-salt challenge (right part of cells, grey border). Cross markers show complete loss (no detection after high-salt challenge) of each species. In all cases but one (shown), baseline *Lactobacillus* populations are no longer detected after high salt intake. **d**, qPCR using *Lactobacillus*-specific 16S rDNA primers in human faecal samples positive for *Lactobacillus* at baseline show a loss of the respective species after 14 days of high salt. *Lactobacillus* 16S rDNA copy number in 4 ng faecal DNA is shown. Symbols indicate study subject, colours indicate respective *Lactobacillus* species. **e**, Kaplan–Meier survival curves contrasting the fate of gut *Lactobacillus* populations (detected using the mOTU framework) following a high-salt challenge (bright red curve) and in healthy control individuals from reference cohorts ($n = 121$, see Methods) not undergoing any intervention (bright blue curve). This is compared with corresponding survival curves over time for the set of all other detected gut bacterial species following high-salt challenge (high salt others, dark red curve) and without challenge in controls (NSD others, dark blue curve). **f**, For a clearer view of its time range, only the salt intervention curves from **e** are shown. Two observations are clear. First, *Lactobacillus* on average persist for shorter times in the gut than the average of all other species. Second, a high-salt challenge strongly increases gut loss of both *Lactobacillus* and non-*Lactobacillus* species. As such, in combination, *Lactobacillus* loss is highly pronounced after high-salt intervention and significantly ($P < 1.62 \times 10^{-8}$) faster than the average of all species. **g**–**i**, Metagenome analysis shows introduction of novel *Lactobacillus* gut populations during human high-salt challenge. All subjects (*x* axis) for which gut *Lactobacilli* were detected following high-salt challenge are shown, and all species detected (*y* axis) using the SpecI (**g**), mOTU (**h**) or MetaPhlAn (**i**) analysis are shown. Heat map cells show abundance (insert counts as fraction of sample total for SpecI and mOTU) and average coverage (reads per position for MetaPhlAn) of the *Lactobacillus* species at baseline (left part of cells, black border) and after high-salt challenge (right part of cells, grey border). Cross markers show novel introduction (no detection at baseline) of each species.

Corresponding Author: Prof. Dominik N. Müller

Date: Sep 25, 2017

Life Sciences Reporting Summary

Nature Research wishes to improve the reproducibility of the work we publish. This form is published with all life science papers and is intended to promote consistency and transparency in reporting. All life sciences submissions use this form; while some list items might not apply to an individual manuscript, all fields must be completed for clarity.

For further information on the points included in this form, see Reporting Life Sciences Research. For further information on Nature Research policies, including our data availability policy, see Authors & Referees and the Editorial Policy Checklist.

Experimental design

1. Sample size

   Describe how sample size was determined.

   Power calculation is a prerequisite for any animal experiment according to the local animal law and was performed using G*Power Software Version 3.1.9.2. Effect sizes were calculated from previously published experiments.

2. Data exclusions

   Describe any data exclusions.

   Data exclusion criteria were pre-established. Technical failures were excluded. Outliers were excluded only after statistical testing. Outlier testing was performed using Grubbs' test (see statistics in Methods section).

3. Replication

   Describe whether the experimental findings were reliably reproduced.

   All findings shown have been reproduced in at least two independent experiments. The number of replicates is given in the respective figure legends. Individual values are shown in each figure.

4. Randomization

   Describe how samples/organisms/participants were allocated into experimental groups.

   Animals were randomly assigned to the respective body weight matched groups. For the clinical studies, participants were included if pre-specified exclusion criteria were absent. Randomization was not necessary for the clinical study because of the absence of different treatment groups (prospective longitudinal design).

5. Blinding

   Describe whether the investigators were blinded to group allocation during data collection and/or analysis.

   Animals were randomly assigned to the respective body weight-matched groups, probiotic and control treatment were administered without knowledge of the treatment groups. The human pilot study was performed in an unblinded manner. Data analysis was performed by the investigators without knowledge of the treatment groups or treatment phase, respectively.

Note: all studies involving animals and/or human research participants must disclose whether blinding and randomization were used.

6. Statistical parameters

For all figures and tables that use statistical methods, confirm that the following items are present in relevant figure legends (or the Methods section if additional space is needed).

n/a	Confirmed	
☐	☒	The exact sample size (*n*) for each experimental group/condition, given as a discrete number and unit of measurement (animals, litters, cultures, etc.)
☐	☒	A description of how samples were collected, noting whether measurements were taken from distinct samples or whether the same sample was measured repeatedly.
☐	☒	A statement indicating how many times each experiment was replicated
☐	☒	The statistical test(s) used and whether they are one- or two-sided (note: only common tests should be described solely by name; more complex techniques should be described in the Methods section)
☒	☐	A description of any assumptions or corrections, such as an adjustment for multiple comparisons
☐	☒	The test results (e.g. *p* values) given as exact values whenever possible and with confidence intervals noted
☐	☒	A summary of the descriptive statistics, including central tendency (e.g. median, mean) and variation (e.g. standard deviation, interquartile range)
☐	☒	Clearly defined error bars

See the web collection on statistics for biologists for further resources and guidance.

Software

Policy information about availability of computer code

7. Software

Describe the software used to analyze the data in this study.

We state and cite all packages and software tools in the Methods section. Statistical analysis was performed using GraphPad Prism 6 and R (Version 3.1.1 R Foundation, Vienna, Austria) using the packages 'lme4' and 'nlme'. Furthermore the R 'survival', 'vegan', 'ape'; Python's scikit-learn module. Code used for the 16S rDNA data analysis has been uploaded to a github repository (https://github.com/almlab/analysis-salt-responsive). Software was obtained from publicly available sources; papers describing the software are cited in the text.

For all studies, we encourage code deposition in a community repository (e.g. GitHub). Authors must make computer code available to editors and reviewers upon request. The *Nature Methods* guidance for providing algorithms and software for publication may be useful for any submission.

Materials and reagents

Policy information about availability of materials

8. Materials availability

Indicate whether there are restrictions on availability of unique materials or if these materials are only available for distribution by a for-profit company.

No unique materials have been used.

9. Antibodies

Describe the antibodies used and how they were validated for use in the system under study (i.e. assay and species).

Antibodies used for mouse flow cytometry analysis: aCD3ε-FITC clone 17A2, aCD3ε-VioBlue clone 17A2, aCD4-APC-Vio770 clone GK1.5, aCD4-Pacific Blue/FITC clone RM4-5, aCD25-VioBlue/FITC clone 7D4, aFoxP3-PerCP-Cy5.5 clone FJK-16s, aIFN-γ-PE-Cy7/APC clone XMG1.2 PE-Cy7/APC, aIL-17A-PE clone eBio17B7, aRORγt-APC clone REA278. Antibodies used for human flow cytometry analysis: aCD3-PerCP-Vio700 clone BW264/56, aIL-17A-APC-Vio770 clone CZ8-2361, aTNF-α-eFlour450 clone Mab11. Antibodies are also described in the Methods section. Specificity of the antibodies has been validated by using isotype controls and FMO controls.

10. Eukaryotic cell lines

a. State the source of each eukaryotic cell line used.

No eukaryotic cell lines were used, ony primary murine cells.

b. Describe the method of cell line authentication used.

No eukaryotic cell lines were used, ony primary murine cells.

c. Report whether the cell lines were tested for mycoplasma contamination.

No eukaryotic cell lines were used, ony primary murine cells.

d. If any of the cell lines used in the paper are listed in the database of commonly misidentified cell lines maintained by ICLAC, provide a scientific rationale for their use.

No commonly misidentified cell lines were used.

Animals and human research participants

Policy information about studies involving animals; when reporting animal research, follow the ARRIVE guidelines

11. Description of research animals

Provide details on animals and/or animal-derived materials used in the study.

All animal experiments have been approved by local authorities, registration numbers are given in the Methods section. The following inbred mouse species were used: FVB/N, C57BL/6J. Supplier and age (10-12 weeks) of the mice as well as housing conditions are provided for each experiment in the Methods section. Only male mice were used.

Policy information about studies involving human research participants

12. Description of human research participants

Describe the covariate-relevant population characteristics of the human research participants.

Only healthy male participants were recruited. Study population was homogeneous with regard to age, ethnicity, socioeconomic status, weight, BMI, diet (omnivore) and blood pressure. Baseline characteristics are shown in the Supplementary Information, Table 1.

Corresponding Author: Dominik N. Müller

Date: Sep 25, 2017

Flow Cytometry Reporting Summary

Form fields will expand as needed. Please do not leave fields blank.

Data presentation

For all flow cytometry data, confirm that:

☒ 1. The axis labels state the marker and fluorochrome used (e.g. CD4-FITC).

☒ 2. The axis scales are clearly visible. Include numbers along axes only for bottom left plot of group (a 'group' is an analysis of identical markers).

☒ 3. All plots are contour plots with outliers or pseudocolor plots.

☒ 4. A numerical value for number of cells or percentage (with statistics) is provided.

Methodological details

5. Describe the sample preparation.	Murine cells were isolated from the spleens and intestines as described in the Methods section. Human PBMC were isolated from peripheral venous blood as described in the Methods.
6. Identify the instrument used for data collection.	BD FACSCanto II system
7. Describe the software used to collect and analyze the flow cytometry data.	BD FACSDiva software was used for data collection and FlowJo v10 for data analysis.
8. Describe the abundance of the relevant cell populations within post-sort fractions.	Purity of the sorted T cell fractions was confirmed by flow cytometry resulting in a purity of the sorted cells of >95%.
9. Describe the gating strategy used.	A representative plot and gating is provided with every flow cytometry figure.

Tick this box to confirm that a figure exemplifying the gating strategy is provided in the Supplementary Information. ☐